SECTION B. AREA OF REVIEW AND CORRECTIVE ACTION PLAN
40 CFR 146.84(b)

MONTEZUMA CARBON SEQUESTRATION HUB

Facility Information

Facility name: Montezuma Carbon Sequestration Hub
IW-1A

Facility contact: Jim Levine, Managing Partner
2000 Powell Street, Suite 920
Emeryville, CA 94608
Phone: (510) 409-1765
Email: jim.levine@upstream.us.com

Well location: Collinsville, Solano County, California
Lat: 38º5'7.334" N Long: -121º51'30.914" W NAVD 88
Sec 22 T 3 N R 1 E

Table of Contents

List of Tables

List of Figures

List of Appendices

Appendix B-1. Oil and Gas Wells

Appendix B-2. Water Wells

SECTION B. AREA OF REVIEW AND CORRECTIVE ACTION PLAN
40 CFR 146.84(b)

B.1 PLANNED COMPUTATIONAL MODELING

B.1.1 SIMULATOR NAME AND AUTHORS/INSTITUTION

TReactMech V4.213/ECO2N V2

The computational modeling for the MC project is being performed by a team of professionals associated with Lawrence Berkeley National Laboratory (LBNL).

B.1.2 DESCRIPTION OF SIMULATION ALGORITHM

TReactMech is a parallel Thermal-Hydrological-Mechanical-Chemical (THMC) continuum geomechanics simulator based on TOUGHREACT V4.13 OMP (Sonnenthal et al., 2021; Xu et al. 2011), with improvements to the TOUGH2 (Pruess et al., 1999) multiphase flow core. The geomechanical formulation is based on a 3-D continuum finite-element model with full 3-D stress calculations, plastic deformation via shear and tensile failure (Kim et al., 2012; 2015; Smith et al., 2015; Sonnenthal et al., 2018). The TOUGH family of codes use the Integral Finite Difference Method (IFDM) (Edwards, 1972; Narasimhan and Witherspoon, 1976), which is a finite-volume method. It offers great flexibility in grid design including local grid refinement, choice of grids to minimize grid orientation effects, and efficient treatment of heterogeneity including fractured rock. The IFDM has been in use for coupled fluid flow/heat transfer problems for at least 45 years. Code comparison studies have verified its accuracy and robustness, therefore, a comparison of IFDM to another model using a different spatial discretization method is not needed. Doing a grid refinement study is an important part of modeling a given problem and will be conducted for the MC project once the stratigraphic test well has been drilled and data collected. The equation of state (EOS) TOUGH reservoir simulation package ECO2N V2.0 (Pan et al., 2015; Pruess and Spycher, 2007; Spycher and Pruess, 2005) was used to model the CO_2 plume and pressure propagation into the earth. This package considers H_2O, NaCl, and supercritical CO_2 fluid flow and is multi-phase extension to Darcy's law, with inter-phase effects controlled by capillary pressure and relative permeability functions, which may be hysteretic (Doughty, 2007, 2013). Using the capability in ECO2N, solid NaCl salt, or more complex salt mineral assemblages may precipitate from solution (using the reactive-transport capabilities), with reversible changes in porosity, permeability, and capillary pressure.

TReactMech is ideally suited for continuum representations of fractured and porous rock masses at scales of meters to tens of kilometers (Sonnenthal et al., 2018). TReactMech can also simulate processes at the scale of individual fractures, such as for simulating hydraulic fracturing, or single-fracture deformation at the core-scale (Dobson et al., 2021). The continuum model approach considers local (grid-block scale) averaging of fracture porosities and permeabilities. Heat and fluid flow, stress, and reactive transport are solved using the

sequential non-iterative approach. Fluid flow and heat transport are solved simultaneously as in TOUGH2 (Pruess et al., 2012) with modifications to consider multiple coupled geochemical and geomechanical effects on porosity and permeability. TReactMech uses a hybrid parallel computation approach, in which the geomechanics and fluid flow are solved using PetSc/MPI and the reactive chemistry with OpenMP. Geomechanics (3D stress equations, strain and failure strain) are solved after fluid and heat flow, followed by transport of aqueous and gaseous species, mineral-water-gas reactions, and finally permeability-porosity-capillary pressure changes owing to geomechanical and geochemical changes to porosity (or fracture aperture).

The TOUGH codes have been widely used over the past 20 years to study CCS, including scoping and design studies, code comparisons, and analysis of laboratory and field data (Doughty and Myer, 2009; Birkholzer et al., 2012; Pruess et al., 2004; Doughty et al., 2008; Finsterle et al., 2014; Aradóttir et al., 2012).

Geochemical reactions are not considered in the simulations presented in this report. All multiphase simulations are non-isothermal and consider gradients in salinity coupled to density and viscosity, and salt precipitation during dryout.

Dispersion is not included in most members of the TOUGH family of codes, including those used for the present study (TOUGHReact, TReactMech, TOUGH3). Because the model grid covers a large region and given its resolution there is some numerical dispersion. Analysis of macroscopic dispersion caused by porosity/permeability/capillary pressure heterogeneities could be considered once core log data are available to add stochastic variability.

B.1.3 MODEL INPUTS AND ASSUMPTIONS

The geologic/hydrogeologic information that serves as inputs to the model described in detail in the Section A.I Site Characterization portion of the application. This section will describe the specific parameters used for the computer simulations.

Simulation Model Domain

The reservoir model was represented by a 146 × 146 × 148 grid in a Cartesian system with 146 grid points in the x-direction, 146 grid points in the y-direction, and 148 grid points in the z-direction, for a total of 3,154,768 grid points. Model domain information is summarized in Table B-1.

SECTION B. AREA OF REVIEW AND CORRECTIVE ACTION PLAN
40 CFR 146.84(b)

TABLE B-1. MODEL DOMAIN INFORMATION

Coordinate System	State Plane		
Horizontal Datum	NAD27		
Coordinate System Units	ft		
Zone	SPCS27-1201		
FIPSZONE	1,201	**ADSZONE**	3,776
Coordinate of xmin	277,028.18	**Coordinate of xmax**	408,692.78
Coordinate of ymin	1,103,729.25	**Coordinate of ymax**	1,235,364.89
Coordinate of zmin	-7113.19	**Coordinate of zmax**	-4272.78

Model Geometry

The model dimensions were 6 km E/W by 18 km N/S with the injection well located in the center of the model. No-flow boundaries are applied at all model boundaries, except at the top of the full model, which represents the atmosphere. The 6 km E/W distance was selected to create a no-flow boundary at the projected distance between Kirby Hills Fault at the Anderson level and the injection well. As described in the Section A.I Site Characterization portion of the application, the Kirby Hills Fault traps gas on the east side of the fault and possesses sealing upper Cretaceous shales on the west side of the fault. The grid resolution is variable, with finest resolution around the injection well (25 m). The figure below shows a cut-away view of the model, illustrating the gridding. The Anderson reservoir was 396.3 m thick, with 16 layers, each 24.77 m. The lateral grid resolution at the injection well is 25 m. Examples of the 3-D grid (with cut-way), rock units, and permeability with a CO_2 plume at various times are shown in Figure B-1.

FIGURE B-1. EXAMPLES OF 3-D RESERVOIR MODEL GRID (TOP) AND PERMEABILITIES (BOTTOM) SUPERIMPOSED CO_2 PLUME AT 30 AND 40 YEARS

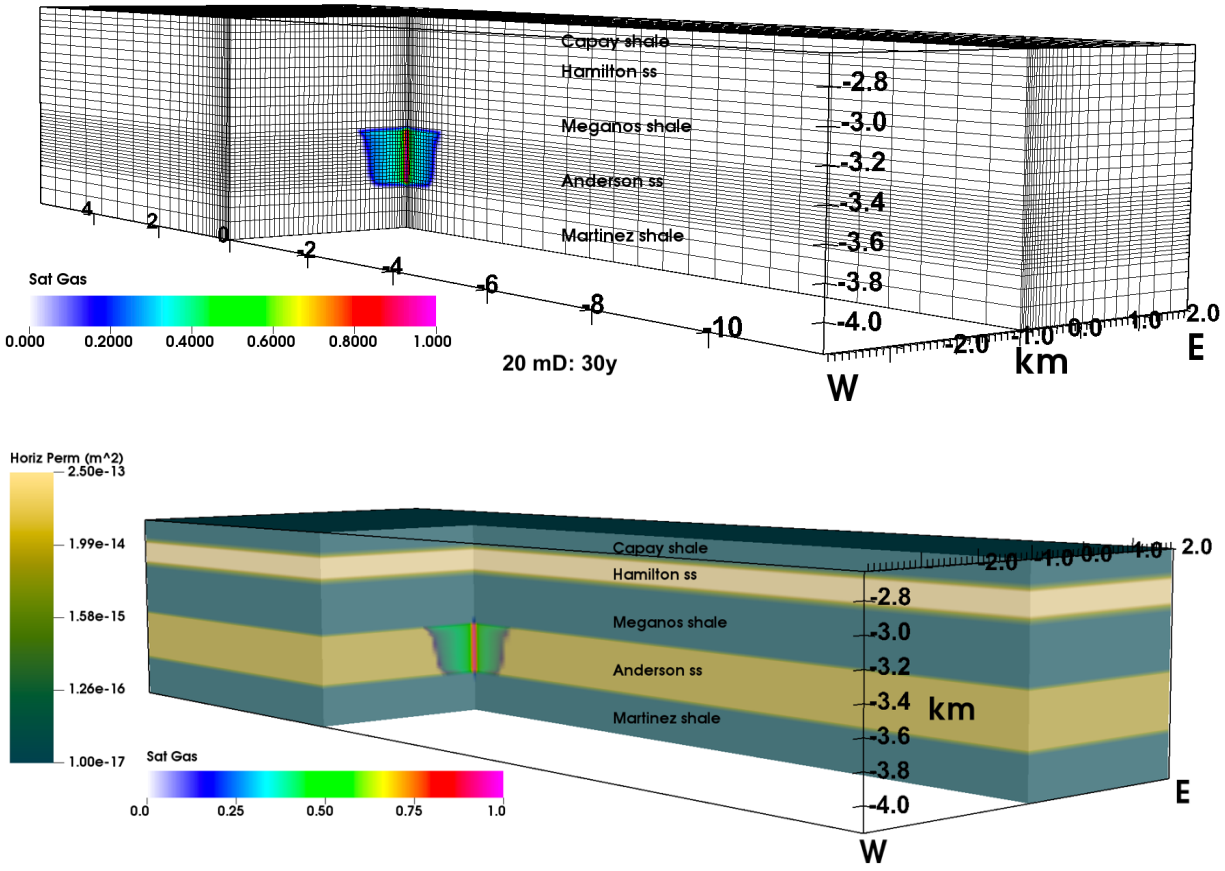

Reservoir Initial Conditions

An initial hydrostatic pressure gradient, geothermal temperature gradient, and given salinity gradient are specified for a 1D column model extracted from the full model, and the model is allowed to come to steady-state (1 million years). Pressure, temperature, and salinity are fixed at the top of the model (the ground surface), and temperature is fixed at the base of the model. The temperature difference between model top and bottom corresponds to a geothermal gradient of 22.7 ºC/km. The initial salinity gradient is 3350 ppm/km, which was estimated from local literature values. Initial dissolved CO_2 concentrations were assumed to be uniformly 100 ppm. The 1-D steady-state temperature, pressure, salinity, and dissolved CO_2 profiles were used as initial conditions for the 3-D reservoir models. The 3-D models were then run for 10,000 years to a new steady-state to account for any local convective (thermo-haline circulation) effects.

SECTION B. AREA OF REVIEW AND CORRECTIVE ACTION PLAN
40 CFR 146.84(b)

Initial conditions at the top of the Anderson reservoir were as follows:

- Top of Reservoir: 3456.6 m
- Reservoir Temperature: 96.46 ^{o}C
- Reservoir pressure 33.82 MPa
- Reservoir salinity 16,658 ppm
- Fluid density 987.27 kg/m^3
- Permeability (20mD, and a second run at 200 mD)
- Porosity 20%

Hydrological and Thermal Parameters - Hydrological and thermal properties are given for the 3-D reservoir model in Table B-2. Unsaturated hydrologic properties (capillary pressure and relative permeability) for the van Genuchten (P_{cap}) and van Genuchten-Corey models are generic values for sandstones and shales based on the user's guides for the modeling software. Thermal conductivities (bulk, kT) and grain heat capacities (Cp) are also generic values for sandstones and shales. Note that the permeabilities of the units were given anisotropy ratios (vertical/horizontal) of 0.1 for shales and 0.2 for sandstones to account for internal layering and heterogeneity not considered directly.

TABLE B-2. HYDROLOGICAL AND THERMAL PROPERTIES FOR THE 3-D RESERVOIR MODEL.

Rock	*kh,kv* (mD)	ϕ	K-rel	λ	S_{lr}	S_{ls}	S_{gr}	Pc ap	λ	S_{lr}	$1/P_0$ Pa^{-1}	k_T (w, d) $W\ m^{-1}\ K^{-1}$	Cp $J\ kg^{-1}\ C^{-1}$
Capay shale	0.01 0.001	0.20	VG-C	0.412	0.2	1.	0.05	VG	0.412	0.0	$5.32x10^{-5}$	2.0, 1.5	900.
Hamilton sandstone	250 50	0.19	VG-C	0.400	0.2	1.	0.05	VG	0.400	0.2	$2.79x10^{-4}$	2.5, 1.875	900.
Meganos/ Upper Martinez shale	0.01 0.001	0.20	VG-C	0.412	0.2	1.	0.05	VG	0.412	0.0	$5.32x10^{-5}$	2.0, 1.5	900.
Anderson sandstone	20, 200 4, 40	0.20	VG-C	0.400	0.2	1.	0.05	VG	0.400	0.2	$2.79x10^{-4}$	2.5, 1.875	900.
Lower Martinez shale	0.01 0.001	0.15	VG-C	0.400	0.2	1.	0.05	VG	0.400	0.0	$5.32x10^{-5}$	2.0, 1.5	900.

VG: Van-Genuchten
VG-C van Genuchten-Corey
kT (w,d) wet, dry thermal conductivities

As shown above, the sensitivity analysis for the modeling focused on varying the reservoir permeability. Once the Pre-Operational Testing Program (e.g., installation and analysis associated with the future stratigraphic test well, 3D seismic imaging) is completed, it will be possible to further constrain the current model and to conduct additional sensitivity analysis. It is anticipated that sensitivity studies will include permeability (especially permeability heterogeneity) and boundary conditions, but any model input not well-constrained by field data will be considered also. A grid refinement study will be done. It will be useful for confirming that the current grid resolution is adequate, but also to examine whether different grid resolutions are appropriate for different model purposes. For example, to examine near-well dryout, geochemical reactions, and possible permeability reduction, a fine grid near the well may be needed. On the other hand, to examine the sensitivity to large-scale heterogeneity and lateral boundary conditions, a coarser grid may be adequate. When fully coupled geomechanics and geochemistry are included, model run-time lengthens considerably, so determining how coarse the model can be is important for obtaining model results in a reasonable time frame.

Injection Conditions

Injection of 1 MMt/year gas at mass fractions of 98% CO_2 and 2% H_2O was spread over the 16 intervals in the Anderson sandstone. An approximate enthalpy of CO_2 at 90°C and 20 MPa ($4.02x10^5$ J/kg) was derived from https://www.ohio.edu/mechanical/thermo/property_tables/CO2/C02_Transcrit2.html. The enthalpy of H_2O at

90°C and 1.01325x10^5 Pa (3.7696x10^5 J/kg) was derived from https://www.thermexcel.com/english/tables/eau_atm.htm.

Simulation Parameters

The 20 mD reservoir simulation was run for 40 years of injection and then 60 additional years without any injection for a total of 100 years. A more permeable case with the Anderson sandstone set to 200 mD was run to 30 years injection. Timestepping in the simulations is dynamic and typically ranged from a few hours to several days.

Operational Information

The injection well was modeled as a column of 16 equal-thickness (24.77 m) grid blocks in the Anderson sandstone with areal extent 25 m by 25 m. The total amount of CO_2 injected (1 million tonnes per year) was divided equally among the grid blocks as mass sources with enthalpy approximately equal to the temperature of the grid block into which it is being injected. The Peaceman (1977) correction was applied to convert the grid-block pressure response to the response at a well with radius 0.3 m. This conversion is only needed for verifying that the maximum operating pressure (determined below) is not exceeded. Table B-3 summarizes the operating details for the modeled injection. Sources for depths and formation pressures are found in Section A.I.5 and Figure A.I-6 of the Site Characterization.

TABLE B-3. OPERATING DETAILS FOR THE MODELED INJECTION WELL

Parameters and units		
Model coordinates (ft; m)	X	0
	Y	0
Injection Interval (ft; m)		11,300 to 12,600 ft; 3,445 to 3,840 m
Wellbore diameter at injection interval (in, m)		11.8; 0.3
Lateral extent of grid block containing well (m)		25
Peaceman (1977) correction for P (psi; Mpa) (for 20 mD case)		20.3 psi; 0.14 Mpa
Injection duration (years)		40
Injection rate (MMT/year)		1.0
Total injection mass (MMT)		40

Parameters and units	
Fracture gradient (psi/ft; kPa/m)	0.71; 16.02
Max. op. pressure (MOP) (psi; Mpa)	7,202; 49.7
Pressure Differential (MOP-Reservoir Pressure) (psi; Mpa)	2,291; 15.8

We chose 0.71 psi/ft = 16.02 kPa/m as the fracture gradient for the simulations, based on lower values of pore pressure (Figure A.I-6) which are consistent with mud weights at nearby deep wells (Anderson 5, McDougal, and GP1-7). Table B-3 summarizes the Maximum Operating Pressure (MOP) based on this fracture gradient and a 90% safety factor. The MOP is equivalent to the bottomhole pressure which includes the hydrostatic head of supercritical CO_2 along with the injection pressure. MOP is 7,202 psi, thus, using a hydrostatic reservoir pressure estimate of 4,902 psi, the maximum injection pressure is 2,291 psi, based on the current model. Using a permeability of 20 mD, a net sand thickness of 910 ft, and an injectivity index of 0.08, yields an estimated maximum CO_2 injection volume into the Anderson of 1.4 Mmtonnes/yr (Valluri, et al., 2021), which provides about 50% more injectivity than is planned.

B.2.2 THERMAL-HYDROLOGICAL-MECHANICAL MODEL

A preliminary analysis of the geomechanical response to CO_2 injection was performed using the initial and final 40-year pressure and temperature distributions from the 20 mD simulation, then solving the resultant 3D stress and thermo-poroelastic strain equations using TreactMech. Fracture generation was not allowed to take place by increasing the cohesion to a large value.

Geomechanical Properties and Boundary Conditions

Geomechanics controls the changes in stress and the potential for fracture generation or stimulation in response to pressure, temperature, and stress changes. In short, in response to changes δP, δT in pressure and temperature, and possible changes in strain δε, and stress δσ changes as

$$\delta\sigma = \mathbf{C}\,\delta\epsilon - \alpha_b \mathbf{I}\,\delta P - 3\,\alpha_{th} K_{dr} \delta T \qquad \text{Eq. 1}$$

where **C** is the stiffness matrix, α_b the Biot coefficient, α_{th} the coefficient of (lineal) thermal expansion, K_{dr} is the drained bulk modulus, and **I** is an identity matrix, where changes in possible failure strain $\delta \varepsilon$) have been (temporarily) neglected. (Here we use a compressive stress negative convention.) Change in strain $\delta \varepsilon$ is found from the requirement that stress satisfy the force balance equation

$$\boldsymbol{\nabla \cdot \sigma} + \boldsymbol{\rho_b} = \mathbf{0} \qquad \text{Eq. 2}$$

Shear failure occurs if

$$\mathrm{F_{ij}} \equiv \boldsymbol{\sigma}_{\mathbf{ii}}^{(\mathbf{pr})}) - \sigma_{jj}^{(pr)} - 2\, C_{sh} \cos\phi_{fr} \quad + \left(\sigma_{ii}^{(pr)} + \sigma_{jj}^{(pr)}\right) \sin\phi_{fr} > \mathbf{0} \qquad \text{Eq. 3}$$

where $\sigma_{11}^{(pr)}$, $\sigma_{22}^{(pr)}\sigma_{33}^{(pr)}$ are principal effective stresses (effective stress components in coordinates in which stress is diagonal), C_{sh} is rock cohesion, and ϕ_{fr} is rock internal friction angle. Tensile failure occurs when the minimum effective exceeds the tensile strength.

We model equations (1-3) for δP, δT from the solution to the multiphase flow. Changes in stress σ, result in (thermoporoelastic) changes in porosity. In general, we model the problem of coupled flow and mechanics with changes in temperature and pressure affecting the mechanics and changes in porosity affecting the flow. However, due to time constraints, in the current work, the coupling of mechanics back to flow was approximated with a pore compressibility term based on rock bulk modulus and changes in pressure; changes in stress and possible material failure were computed from the changes in pressure and temperature without coupling of mechanic back to flow beyond the pore compressibility term.

Bulk moduli under undrained conditions and shear moduli were computed from a model of P wave velocity (Vp) and S wave velocities (Vs) for the West (Sacramento) Delta region (Brocher, 2004), with density computed from a correlation with Vp (loc. Cit.). Bulk moduli were adjusted to drained conditions using Gassman's equation, using the porosities in Table B-2, and estimated grain bulk moduli for sandstones and shales. Sandstones were assumed to have a grain bulk modulus of quartz (37 Gpa). Grain bulk moduli for shales were computed for a 'typical' composition of 58 % clay minerals, 28 % quartz, 6 % feldspar, 5 % carbonates, 2 % iron oxides, with clay minerals portioned as 25% illite, 20 % kaolinite, and 14% smectite, and feldspar treated as plagioclase. The structurally similar biotite bulk modulus was used for the

(unmeasured) illite bulk modulus, following Asaka et al. (2021). Average bulk moduli of harder minerals and of softer minerals (kaolinite and smectite) were computed separately using volumetric reciprocal averaging, and the two averages combined treating the harder mineral component as matrix in an upper Hashin-Strikman bound average, yielding a 44 Gpa estimated shale grain bulk modulus. The resulting elastic moduli under drained conditions are given in Table B-4, as well as Biot coefficients, computed from

$$\alpha_b \equiv 1 - K_{dr} / K_{gr} \qquad \text{Eq. 4}$$

where K_{dr} is drained bulk modulus, and K_{gr} is grain bulk modulus. Material cohesion, and internal friction angles were computed from Vp using correlations estimated for shales and said to also be fairly satisfactory for sandstones (Lai, 1999).

TABLE B-4. GEOMECHANICAL PROPERTIES

Unit	Bulk Modulus (Gpa)	Young's Modulus (Gpa)	Shear Modulus (Gpa)	Poisson's Ratio	Biot coef	Friction Angle (deg)	Cohesion (Mpa)	Tensile Strength (Mpa)	Thermal Expansion Coef (1/°C)
Capay sh	17.5	28.2	11.4	0.232	0.603	36.0	7.3	7.3	1.0×10^{-5}
Hamilton ss	19.8	31.2	12.6	0.238	0.463	36.8	7.5	7.5	1.0×10^{-5}
Meganos/ Upper Martinez sh	21.2	35.6	14.6	0.221	0.518	37.8	7.8	7.8	1.0×10^{-5}
Anderson ss	25.2	42.2	17.3	0.221	0.352	39.2	8.1	8.1	1.0×10^{-5}
Lower Martinez sh	27.0	47.5	19.7	0.207	0.386	40.2	8.5	8.5	1.0×10^{-5}

Initial vertical stresses σ_{zz} were given by vertical loading stress, smoothed laterally. Initial horizontal stresses were set to $\sigma_{hmin} = 1.2\ \sigma_{zz}$, $\sigma_{Hmax} = 1.8\ \sigma_{zz}$, following Foxall et al. (2017). The maximum horizontal stress direction was approximated as North-South, and minimum as East-West. The upper model boundary (top of Capay shale) was given a vertical traction for loading stresses computed for layers above it (57.555 MPa), sides given no normal displacement conditions, allowing upwards and lateral movement, and the lower model boundary no normal displacement conditions.

All geomechanical properties reported above were used in the modeling, except for increases to tensile strength and cohesion for the Thermal-Hydrological-Mechanical Model run described in the next section.

Boundary Conditions

No-flow boundaries are applied at all sides and the bottom model boundaries. The top layer of the full 3-D model represents the atmosphere as a constant-pressure, constant-temperature boundary. For the 3-D reservoir model the top of the Capay shale is treated as hydrostatic (fixed pressure and temperature) with values based on a 1-D steady-state simulation. The lateral boundaries of both the full and reservoir-only model are the same and are as follows:

West: Kirby Hills Fault
East and North: Sherman Island Fault
South: termination of Anderson Formation

Local information (described in Section B.1.3 above) about pressures on opposite sides of the faults suggests that they are closed to flow. The bottom of the full model represents the granitic basement and is assumed to be closed. The reservoir-only model has an open upper boundary and a closed lower boundary to represent the top of the upper sealing layer and the bottom of the lower sealing layer of the storage reservoir, respectively. Although the top of the Capay shale is an open boundary, the vertical permeability of the Capay is set to 0.001 mD, so it is essentially impermeable.

A fully coupled Thermal-Hydrological-Mechanical Model (THM) was run to compare to the uncoupled simulation. Although it used values of tensile strength and cohesion that were in excess of what would be possible for tensile or shear failure, maximum excess pressures in the simulations never exceeded the estimated values for these rocks (8.1 MPa), owing to the relatively high permeabilities (20-200 mD). Future simulations using an updated geological model and core data will utilize the (re)estimated tensile strength and cohesion.

Geochemical analyses and modeling have not been performed. Once data from boreholes are measured (brine chemistry and core/cuttings mineralogy) fully coupled thermal-hydrological-chemical (reactive-transport) and thermal-hydrological-mechanical-chemical (reactive-transport-geomechanical) models will be run to assess the potential for mineral alteration and precipitation in the dryout zone near the well, permeability changes in the reservoir and the extent of mineral and solubility trapping, and the coupled effect on reservoir pressures during long-term injection.

B.3 COMPUTATIONAL MODELING RESULTS

B.3.1 CO_2 PLUME MODELING RESULTS

Results are shown as contour plots for W-E, S-N, and plan view (top of Anderson sandstone) sections at multiple time intervals in Figures B-2 to B-5. The radius of the CO_2 plume for the 20 mD case, shown as gas saturation in Figures B-2 through B-4, is about 1 km after 40 years injection, and 1.3 km after 100 years.

FIGURE B-2A. CO_2 PLUME (GAS SATURATION) W-E CROSS-SECTION FOR 20 MD CASE AT 1, 20,40, AND 100 YEARS

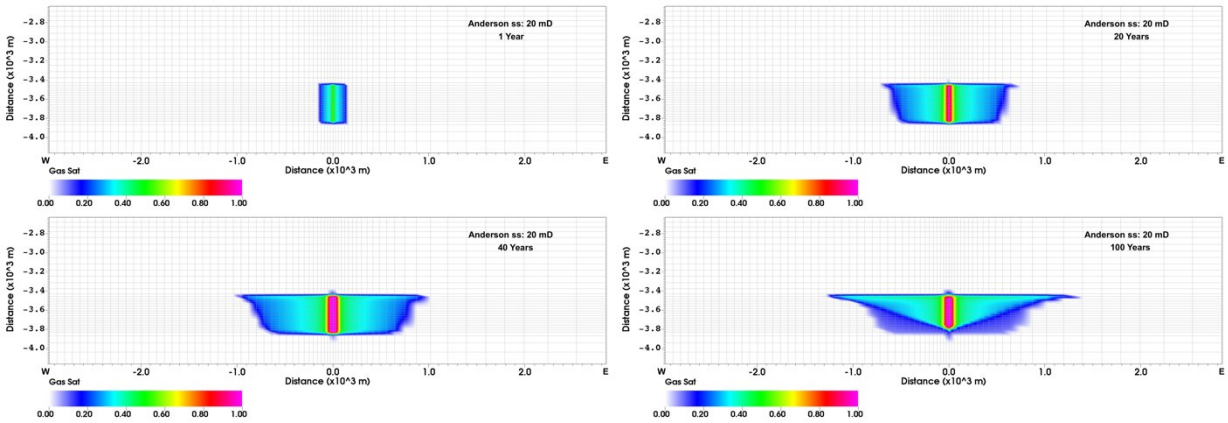

FIGURE B-2B. CO_2 PLUME (GAS SATURATION) W-E CROSS-SECTION FOR 200 MD CASE AT 1 AND 20 YEARS

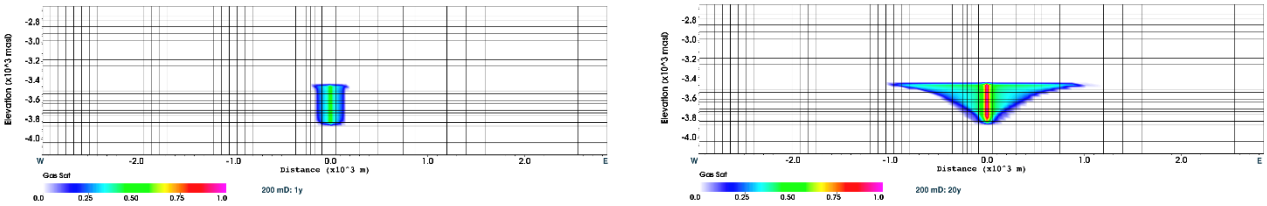

FIGURE B-3. CO_2 PLUME (GAS SATURATION) S-N CROSS-SECTION FOR 20 MD CASE AT 1, 20, 40, AND 100 YEARS

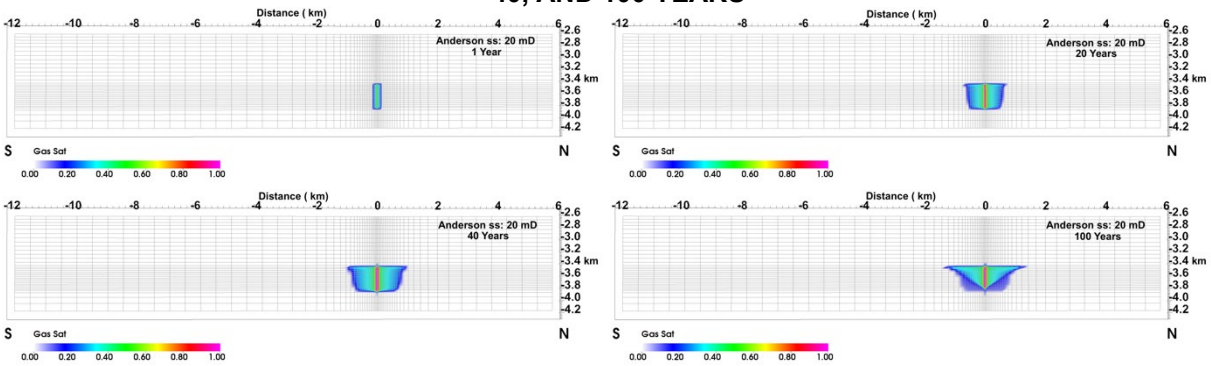

FIGURE B-4A. CO_2 PLUME (GAS SATURATION) AT RESERVOIR TOP FOR 20 MD CASE AT 1, 20, 40, AND 100 YEARS

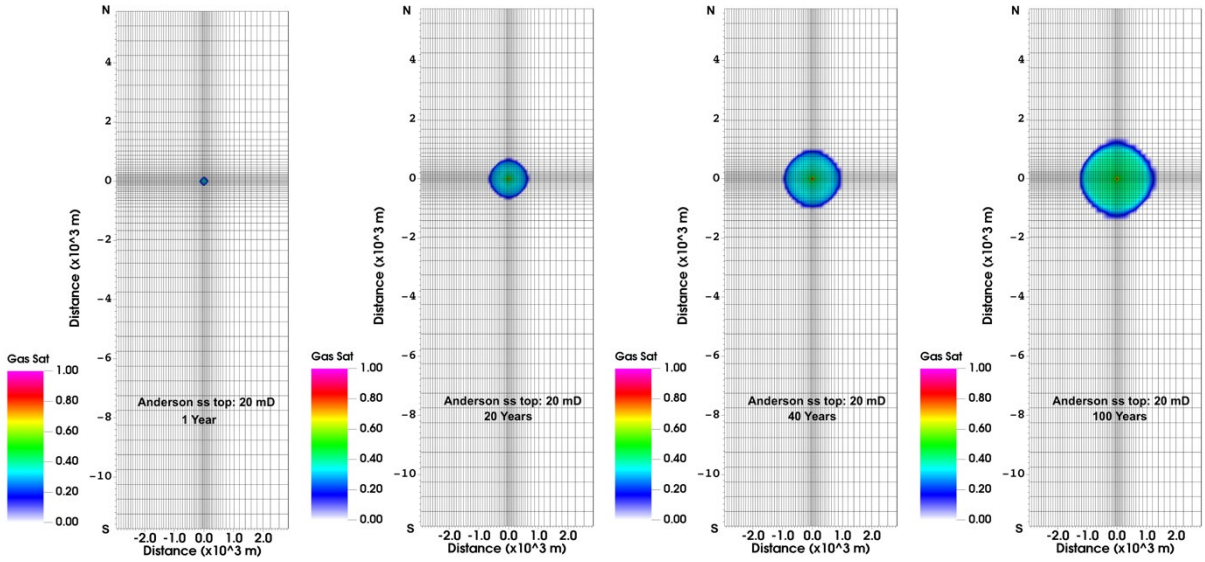

FIGURE B-4B. CO_2 PLUME (GAS SATURATION) AT RESERVOIR TOP FOR 200 MD CASE AT 1 AND YEARS

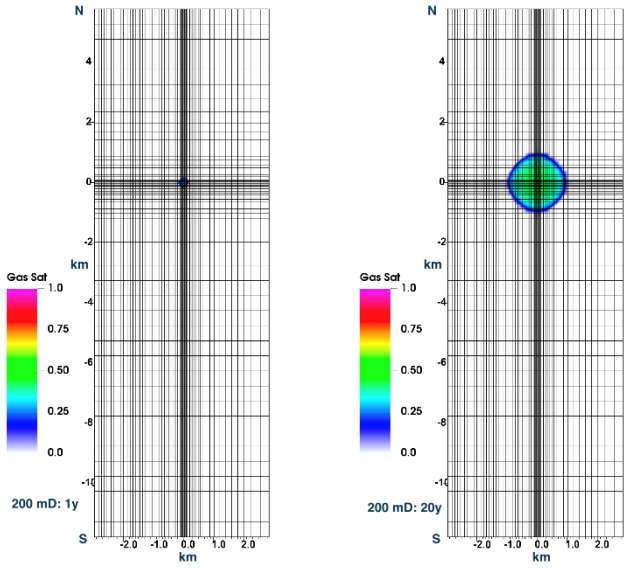

Pressure changes ($P-P_{hydrostatic}$), presented in Figures B-5 through B-6 in two dimensions, show impacts at all boundaries early in the injection period. Figure B-7 includes a comparison of the two permeability cases at 30 years injection. At the Kirby Hills Fault, the 20 mD case estimates about 1.3 MPa after 30 years injection and the 200 mD case estimates about 1.0 MPa.

FIGURE B-5A. NONHYDROSTATIC PRESSURE W-E CROSS-SECTION FOR 20 MD CASE AT 1, 20, 40, AND 100 YEARS

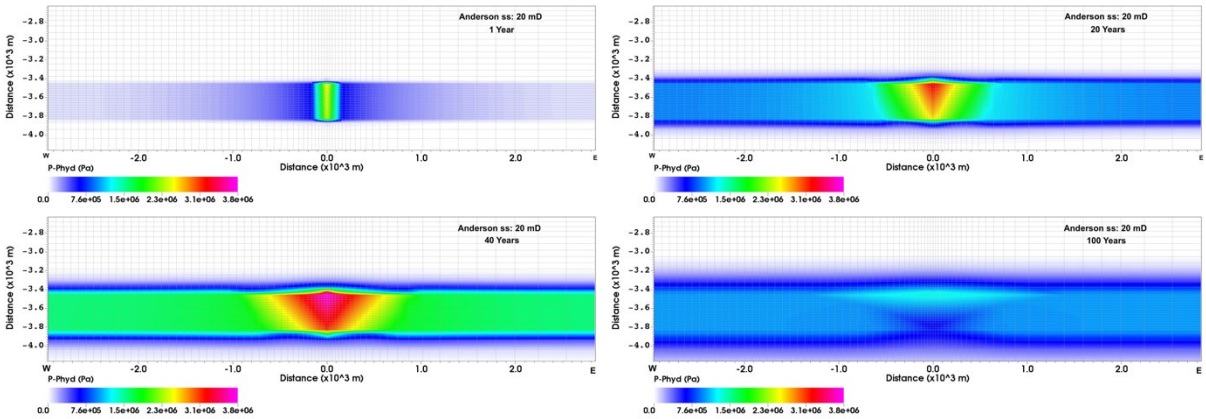

FIGURE B-5B. NONHYDROSTATIC PRESSURE W-E CROSS-SECTION FOR 200 MD CASE AT 1 AND 20 YEARS

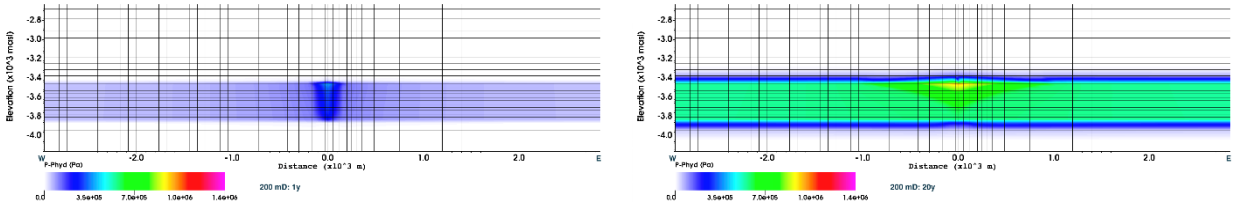

FIGURE B-6A. NONHYDROSTATIC PRESSURE AT RESERVOIR TOP FOR 20 MD CASE AT 1, 20, 40, AND 100 YEARS

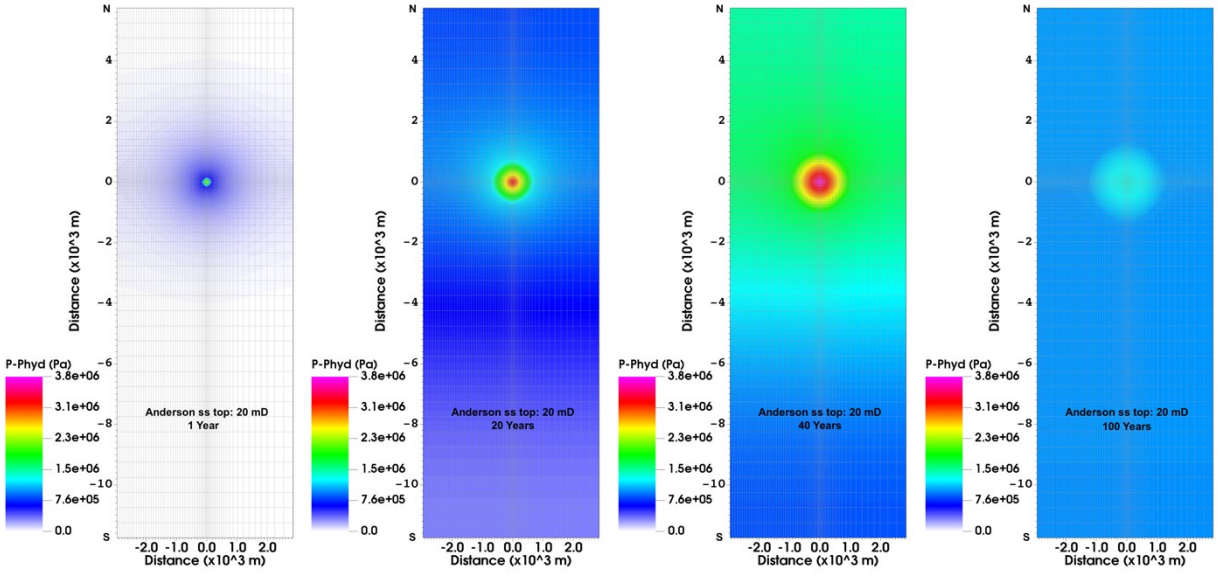

FIGURE B-6B. NONHYDROSTATIC PRESSURE AT RESERVOIR TOP FOR 200 MD CASE AT 1 AND 20 YEARS

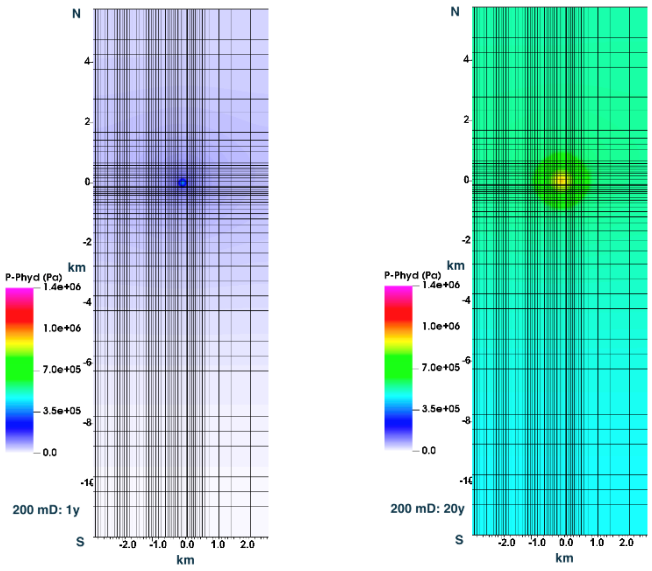

FIGURE B-7. NONHYDROSTATIC PRESSURE W-E AND S-N PROFILES AT RESERVOIR TOP: 20 MD (30 & 40 YEARS) AND 200 MD (30 YEARS)

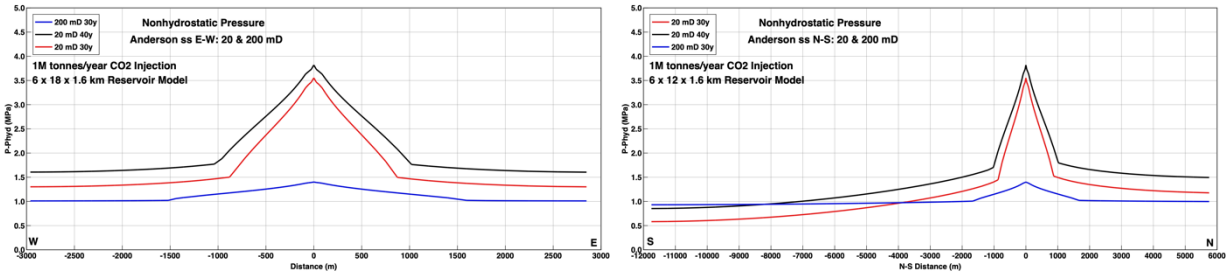

Pressure changes ($P\text{-}P_{hydrostatic}$), shown in Figure B-8, show impacts at the injection well IW-A1 that decrease substantially after injection stops, but remain elevated above background conditions, in the structurally (sealed fault) controlled setting for over 85 years after injection (125 years total).

FIGURE B-8. LONG-TERM PRESSURE CHANGE AT IW-A1 FOR 20 MD CASE AT 125 YEARS

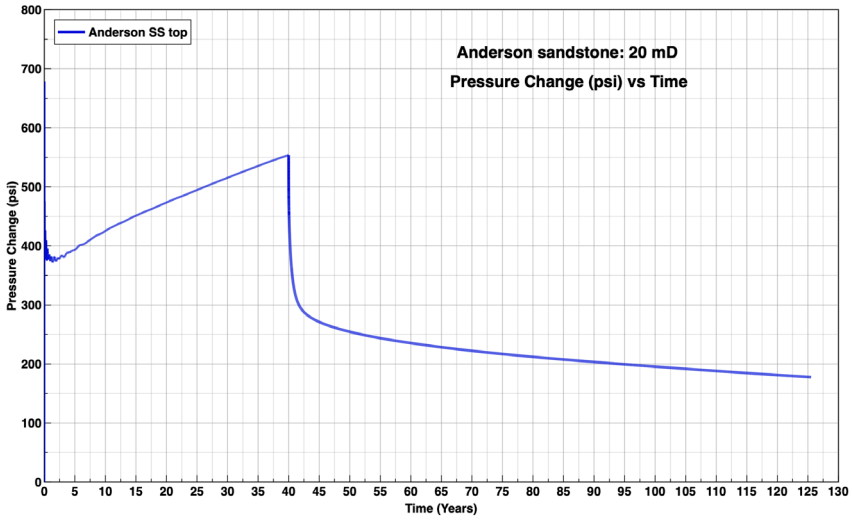

High concentrations of dissolved CO_2 (Figure B-10) extend only about 100 m further than the CO_2 plume after 100 years, and much less at 40 years.

FIGURE B-9. DISSOLVED CO_2 (MASS FRACTION) IN LIQUID SHOWN AT 40 AND 100 YEARS FOR THE 20 MD CASE

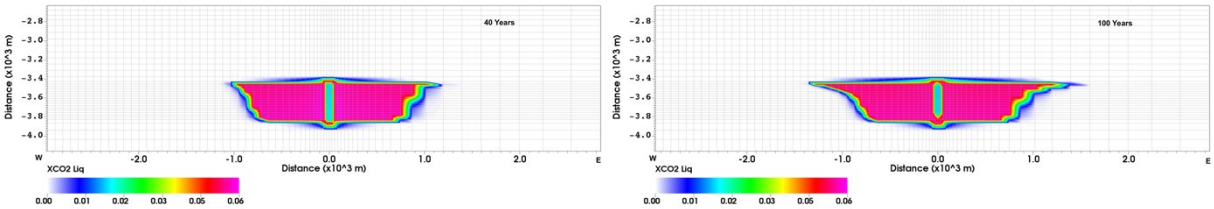

B.3.2 GEOMECHANICAL MODEL RESULTS

The approach used involved calculating the stress changes using the 40 year and initial injection pressures and temperatures (as described above), rather than running the fully coupled simulation for the full time. This method allows for a faster analysis of stress changes, while ignoring potential shear/tensile failure, and other simplifications described above, that may take place during injection.

Profiles of the stress changes for the primary directions from west to east are shown in Figure B-10. Two values of the Biot coefficient for the Anderson sandstone were used, 0.352 (Table B-4) and 0.8 (a conservative value similar to literature values for many sandstones). The higher the Biot coefficient, the higher the stress transferred to the fault, and therefore without site-specific data, a high and low value were considered. The plot shows the stress changes as generally positive (compressive). Although TReactMech by convention

considers compressive stress as negative, the positive stress change with increasing fluid pressure is more intuitive and is plotted that way here.

FIGURE B-10. PROFILES OF THE STRESS CHANGES FOR THE PRIMARY STRESS COMPONENTS FROM WEST TO EAST AT 40 YEARS FOR THE 20 MD CASE

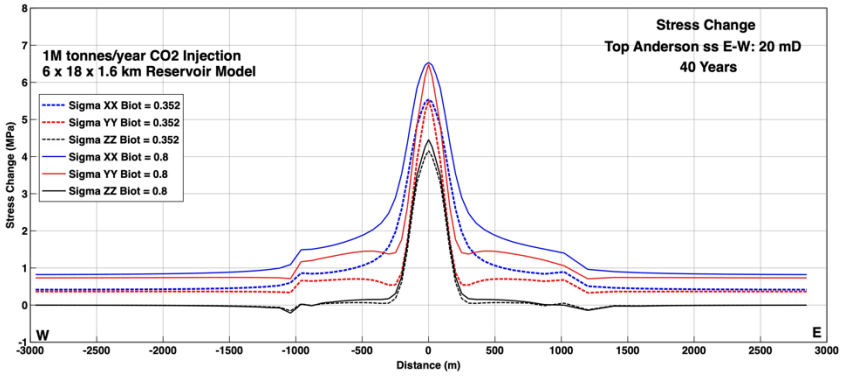

The greatest stress changes are evident at the plume center (~ 6.5 MPa) with up to about an 0.8 MPa increases at the west and east boundaries (σ_{xx}) for Biot coefficient equal to 0.8. Prior to injection σ_{xx} was the intermediate stress and minimum value in the horizontal plane (SHmin).

Cross-sections of the stress contours are shown in Figure B-11. The contour plots are directly from the code output for which compressive stresses are by convention negative, hence the plots show primarily negative stresses. Horizontal stresses (σ_{xx}) show the increased stress confined to the Anderson sandstone. Vertical stress changes (σ_{zz}) propagate a few hundred meters above and below the Anderson sandstone but are confined laterally to the plume region.

FIGURE B-11. CONTOURS OF STRESS CHANGES FOR THE PRIMARY COMPONENTS (DELTA σ_{xx}, DELTA σ_{zz}) FROM WEST TO EAST AT 40 YEARS FOR THE 20 MD CASE

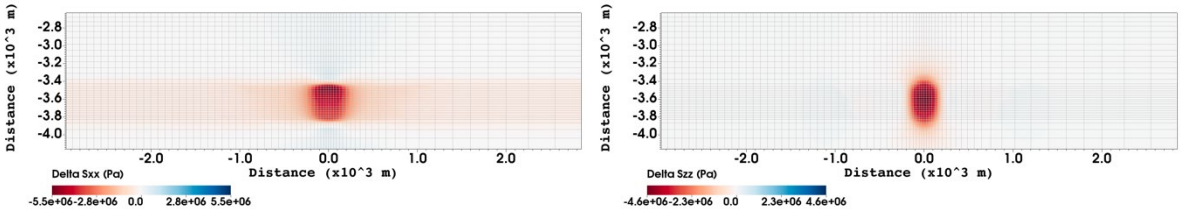

Plan views of the stress contours at the top of the Anderson sandstone are shown in Figure B-12. Over the 40 year period, the stress changes are generally similar in shape to the plume, with some stretching in W-E direction of the σ_{xx} stresses owing to the closer location of the boundaries (faults) and the asymmetric initial stress conditions.

FIGURE B-12. PLAN VIEWS OF STRESS CHANGE (DELTA σ_{xx}, DELTA σ_{zz}) CONTOURS AT THE TOP OF THE ANDERSON SANDSTONE

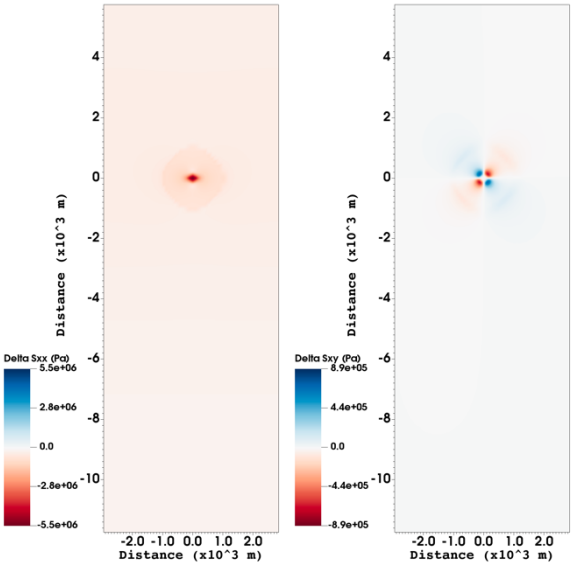

Future work - As improved information becomes available from site characterization and reservoir monitoring data, updated simulations will be performed, including coupled THMC simulations of pressure driven stress, strain, and MEQs coupled to geochemical and geomechanical changes in porosity, permeability, and capillary pressure.

B.4 AoR DELINEATION

To delineate the pressure front, the minimum or critical pressure necessary to reverse flow direction between the lowermost USDW and the injection zone—and thus cause fluid flow from the injection zone into the formation matrix—must be calculated. We use the guidance provided in the May 2013 version (EPA 816-R-13-005) of the *UIC Program Class VI Well Area of Review Evaluation and Corrective Action Guidance* for the case when the deepest USDW and the storage reservoir are in hydrostatic equilibrium (Method 2). Because density in the storage formation is lower than density in the USDW, EPA's Equations 3 and 4, which come from Nicot et al. (2008) Equation 7, cannot be used. Instead, we use Nicot et al.'s Equation 9, as presented in Bandilla et al. (2012), in conjunction with 1D numerical modeling. The equation for critical pressure change (increase over original pressure) is

$$\Delta P_{crit} = gdz\left[\frac{(\lambda-\xi)}{2}dz + \rho_{ct} - \rho_w\right], \qquad \text{(Eq. 5)}$$

where
$\xi = \frac{\rho_b - \rho_w}{dz}$, $\lambda = \frac{\rho_{cb} - \rho_{ct}}{dz}$,

and g, acceleration due to gravity, 9.8 m/s^2.

The variables are illustrated in the figure below, but *dz* is used instead of *l* for the distance between the bottom of the USDW and the top of the storage formation.

FIGURE B-13. CONCEPTUAL SKETCH OF DENSITY DISTRIBUTION IN A BOREHOLE (NOT TO SCALE)

K.W. Bandilla et al. / International Journal of Greenhouse Gas Control 8 (2012) 196–204

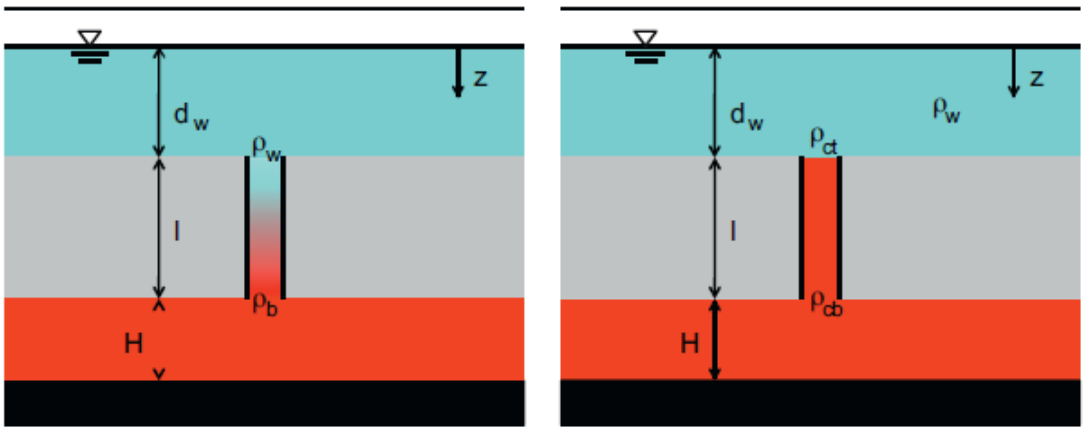

(a) before injecting (b) at critical pressure

The variable ρ is fluid density, which is determined by running 1D column numerical models with TOUGH, for the scenarios in Figures B-13 (a) and (b) above. The 1D columns are extracted from the full model. For Figure B-13(a), initial hydrostatic pressure gradient, geothermal temperature gradient, and given salinity gradient are specified, and the model is allowed to come to equilibrium. Pressure, temperature, and salinity are fixed at the top of the model (the ground surface), and temperature is fixed at the base of the model (basement rock). The temperature difference between model top and bottom corresponds to a geothermal gradient of 22.7 °C/km. The initial salinity gradient is 3,349.5 ppm/km, which is estimated from local literature values. For Figure B-13(b), the initial salinity for the entire depth interval *dz* is set to ρ_b from the Figure B-13(a)

simulation, diffusion is turned off, so salinity remains nearly constant, and the simulation is allowed to come to equilibrium. Table B-5 summarizes the TOUGH simulation results.

TABLE B-5. SUMMARY OF PARAMETERS USED TO DETERMINE CRITICAL PRESSURE, TAKEN FROM 1D COLUMN MODELS

Figure 1a	Grid *z* (m)	P_0 (MPa)	T_0 (C)	Salinity (ppm)	Fluid density (kg/m^3)	Bandilla variable name
Figure 1a - normal steady state						
Tehama Bottom	-590	5.882	32.521	2,744	998.862	ρ_w
Anderson Top	-3456.6	33.82	96.456	16,658	987.274	ρ_b
Figure 1b - constant salinity between reservoir and USDW steady state						
Tehama Bottom	-590	5.886	32.522	16,468	1007.878	ρ_{ct}
Anderson Top	-3456.6	33.95	96.459	16,656	987.331	ρ_{cb}

With the above values for ρ_w, ρ_b, $\rho_{ct,}$ and $\rho_{cb,}$ and using dz = 2866.6, Equation (5) yields ΔP_{crit} = 0.127 MPa.

The AoR is delineated as the greatest extent covered by the combination of the plume and pressure fronts at the time of complete stabilization for the sequestered CO_2. The plume-based component of the AoR is defined by the boundary that encompasses the injected free-phase CO_2 with a concentration greater than 1%. The pressure-front contribution to the AoR is defined by the critical pressure calculations. Based on the preliminary modeling analyses and influenced by the closed boundary assumptions, the pressure front extends outward from IW-A1to the sealed faults to the north, west, and eastern sides of the MC project site. There is some uncertainty about the nature of the Antioch fault south of the project and on the other side of the Sacramento River. However, the closed boundary case currently employed results in the highest pressure increase due to CO_2 injection of all possible boundary conditions (closed, open, partially open, and infinite-acting) due to much smaller extent of the CO_2 plume in comparison to the pressure front. Furthermore, because the extent of the CO_2 plume is so far away from all of the boundaries (including the southern boundary), converting the southern boundary from closed to open is less likely to impact the extent of the CO_2 plume than if the plume extended near the boundary. Figure B-14 shows the plume-based contribution, the pressure-front contribution to the AoR, and the resulting greatest extent covered by the combination.

FIGURE B-14. MODEL PREDICTED AoR FOR THE MC PROJECT

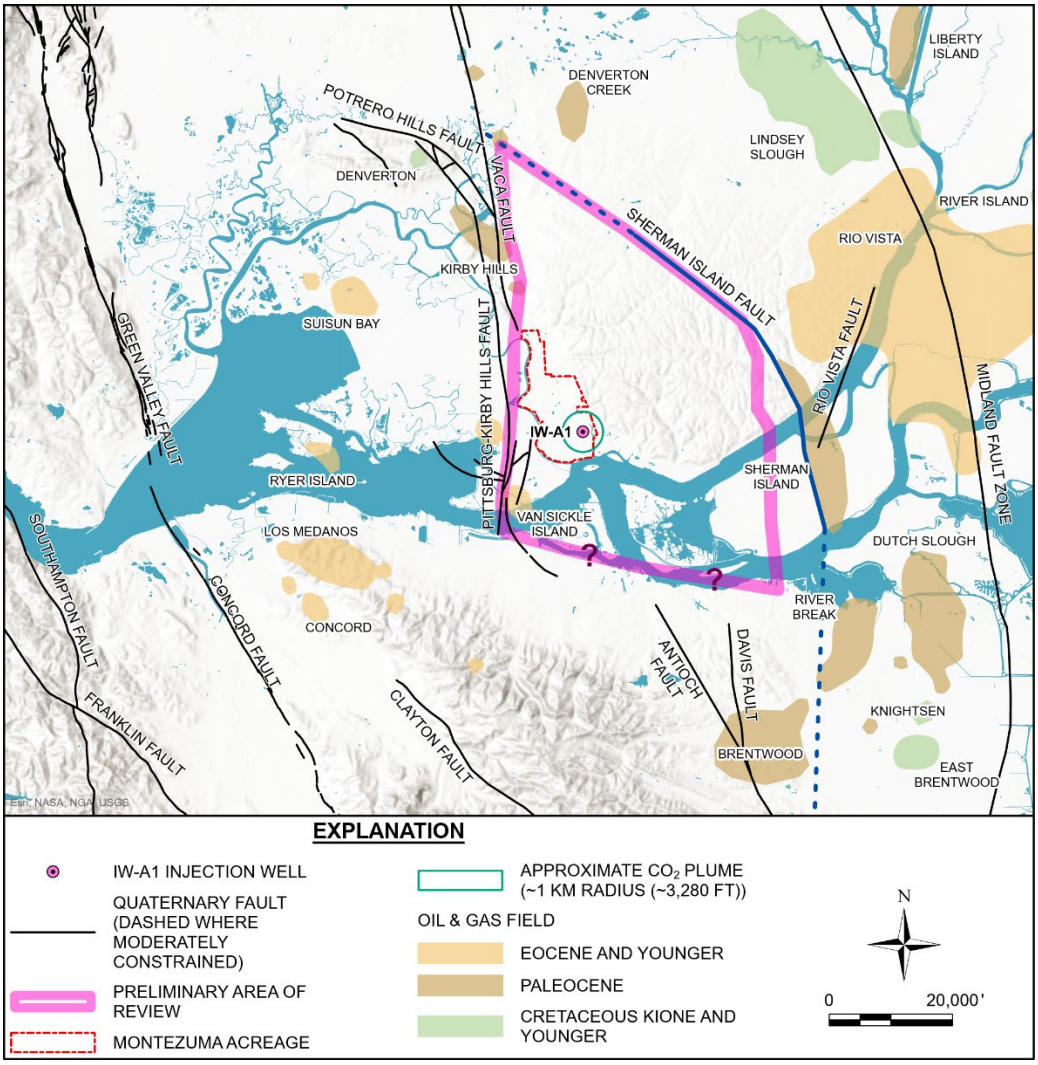

B.5 CORRECTIVE ACTION PLAN AND SCHEDULE

Figures B-15 is a map that displays the location of IW-A1, with idle/legacy oil and gas wells within the areal extent of the AoR. These oil and gas wells are the primary type of artificial penetration of the confining units and injection zone within the AoR and immediate vicinity of the MC project site.

FIGURE B-15. AoR MAP WITH LEGACY OIL AND GAS WELLS

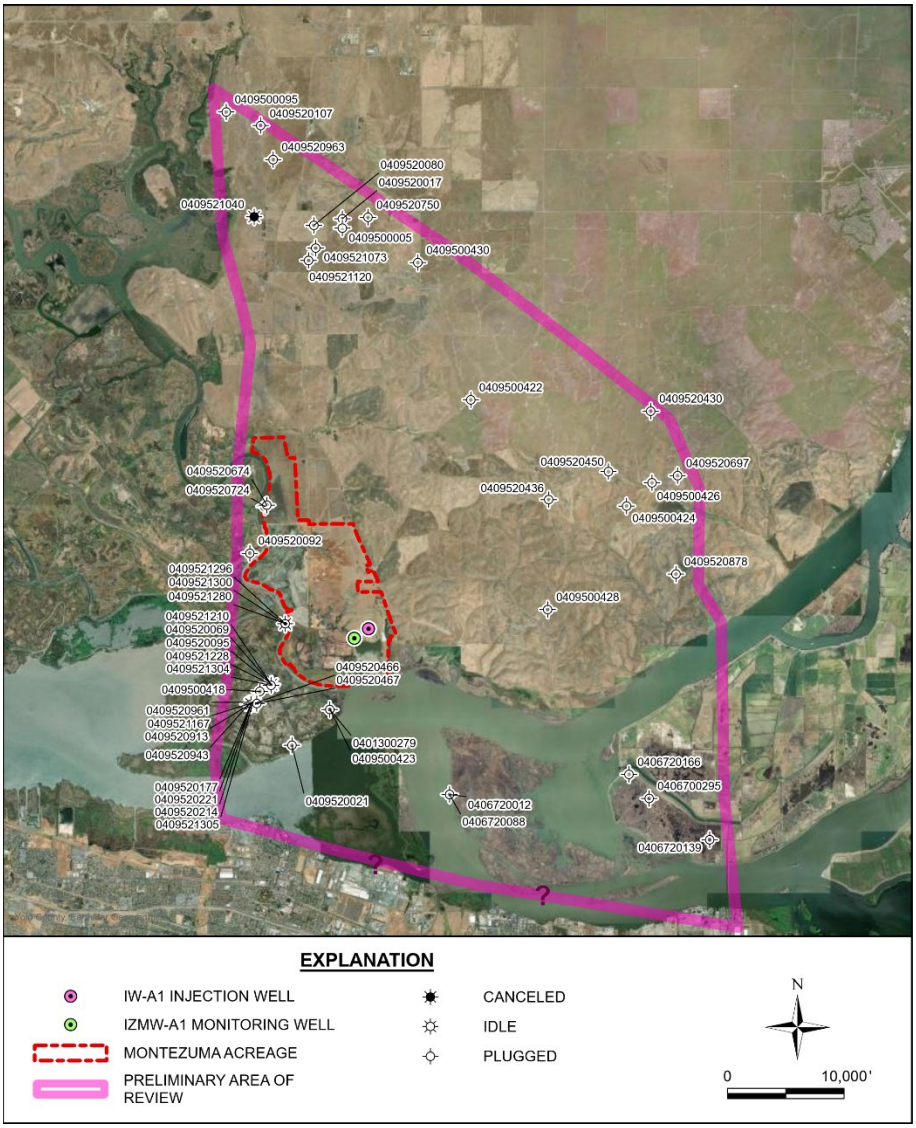

Below is a brief description of relevant research information gathered by MC for other non-well penetrations, none of which were identified as injection zone penetrations within the AoR:

- State- or US EPA-Approved Subsurface Clean-up Sites: PCC searches of the US EPA Cleanups In My Community Map and the database did not result in any candidate penetrations of the confining units or injection zone within the AoR.
- Mine and Quarries (Surface and Subsurface): The MC search of the available public records did reveal a sand dredging/mining operation permitted in Suisun Channel (Figure B-16). Other than this shallow water dredging operation, MC did not identify any other mines and quarries within the AoR or the vicinity of the project site.

SECTION B. AREA OF REVIEW AND CORRECTIVE ACTION PLAN
40 CFR 146.84(b)

FIGURE B-16. AoR MAP WITH WATER WELLS

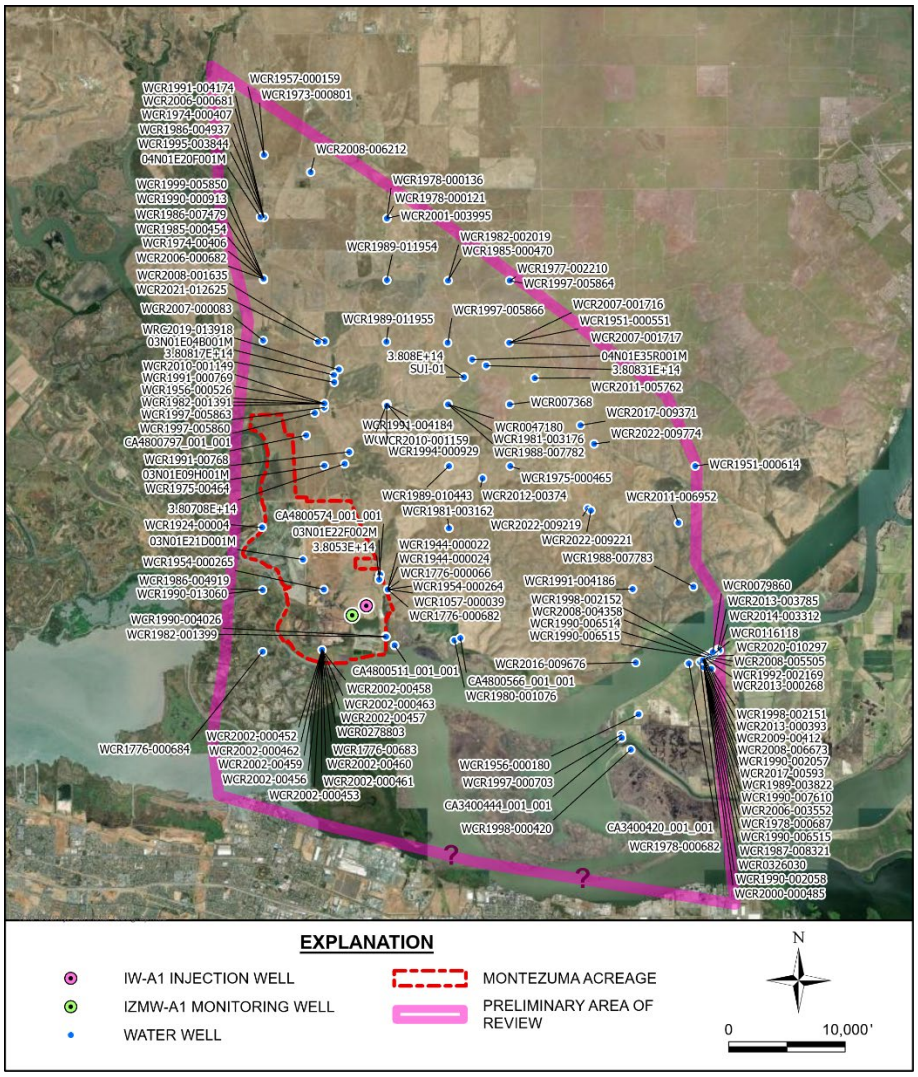

FIGURE B-17. AoR MAP WITH OTHER RELEVANT IDENTIFIED SURFACE AND SUBSURFACE FEATURES

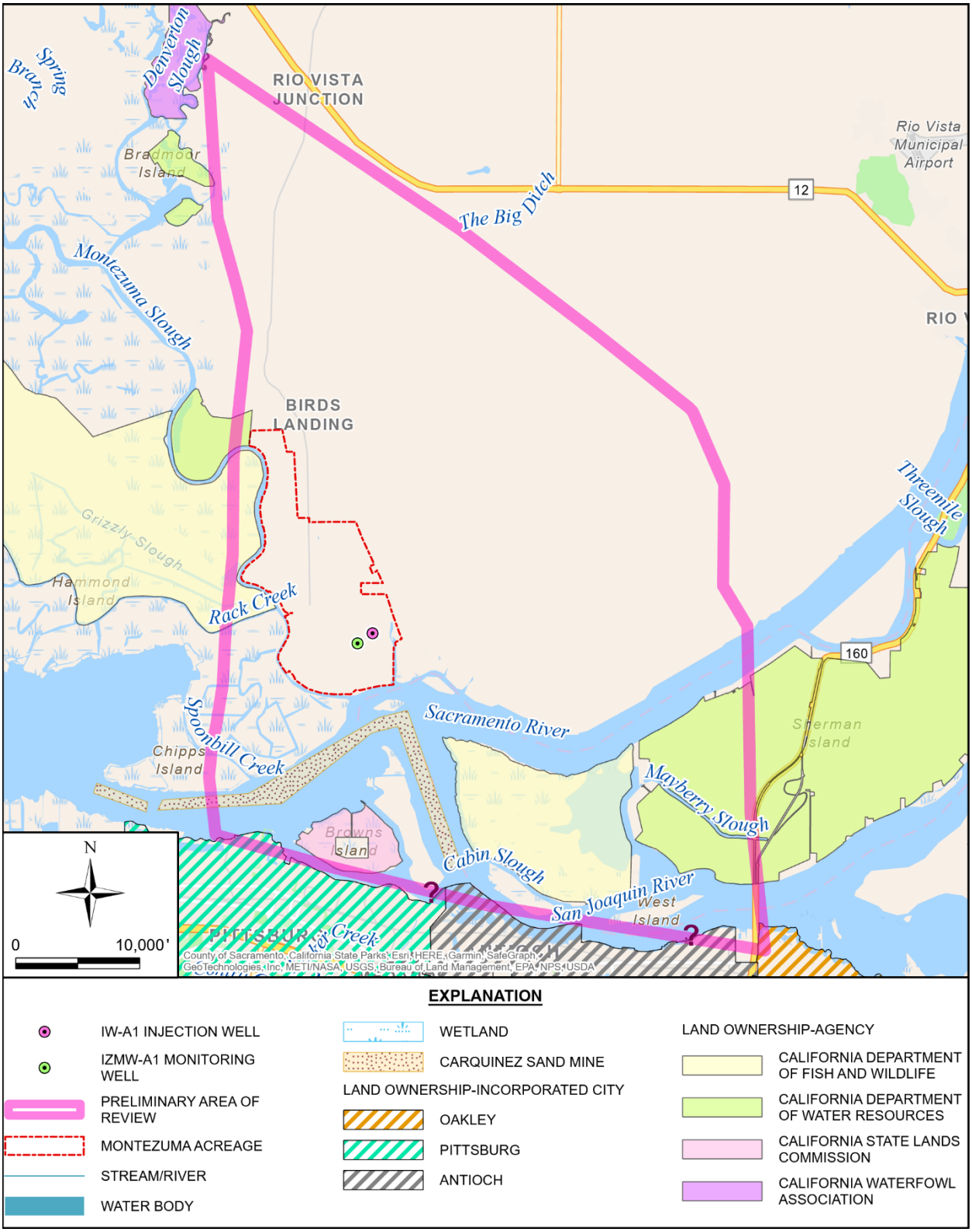

- Faults and Fractures: Multiple sealed faults are identified surrounding the project site and influence and provide structural control of the outer perimeter of the AoR, as previously described. The presence of multiple nearby gas production and storage fields supports the interpretation that these faults function as closed features.

B.5.1. TABULATION OF WELLS WITHIN THE AoR

B.5.1.1. WELL OVERVIEW

MC searched the California Department of Conservation Geology Energy Management Division (CalGEM) Well Finderdatabase, MJ Logs Well Library database, the California Well Sample Repository, the California Natural Resources Agency Department of Water Resources database, and the California Water Boards GAMA Groundwater Information System database in 2023 for wells that may potentially create conduits for fluid movement out of the injection zone. These data are summarized in Appendix B-1 for oil and gas wells and Appendix B-2 for the water wells. Below is a summary of the search findings:

- No Class I, III, IV, or VI wells were identified within the areal extent of the AoR and immediate vicinity.
- Appendix B-1 lists the search findings for 19 oil and gas wellbores that penetrate the top of the Meganos shale upper confining unit within the AoR. Locations of the wells are provided as latitudes and longitudes. The construction of the wells, including conductor pipe, surface casing, and production string is provided in Appendix B-1. The dates drilled for these wells are provided and range from 1943 to 2005. The depths of the wells are provided and range from 4,189 ft to 14,269 ft. The well types are listed as "dry hole or dry gas" in all cases. Finally, all wells except for one (Roaring River 20-2; API ID 09521228) have reported on the table a record of plugging. MC plans to perform a detailed evaluation of these wells.
- For the MC project site, IW-A1 and IZMW-A1 along with any other future CO_2 injection wells proposed for the project site will all be constructed to Class VI standards, thus no corrective actions are needed at this time.
- Appendix B-2 lists search findings for water wells identified within the AoR. The deepest of the wells does not exceed a 800 ft depth, and none of the water wells penetrate the multiple underlying shale units that act as confining units, providing over 9,000 ft of separation between the deepest of these wells and the Anderson Sandstone injection interval. Thus, there is no need for corrective action on any of these wells at this time.

B.5.1.2 WELLS PENETRATING THE CONFINING ZONE (MEGANOS/UPPER MARTINEZ)

Analysis of any wellbore penetrating the confining zone within the areal extent of the AoR will follow the procedures given the US EPA Guidance Document for AoR and Corrective Action (EPA 2013). Figure B-17 is a decision tree that summarizes the analysis procedure. Furthermore, procedures outlined in the guidance document will be followed for any wellbore needing to be re-entered and re-abandoned.

FIGURE B-18. WELL EVALUATION DECISION TREE

From: EPA 2013

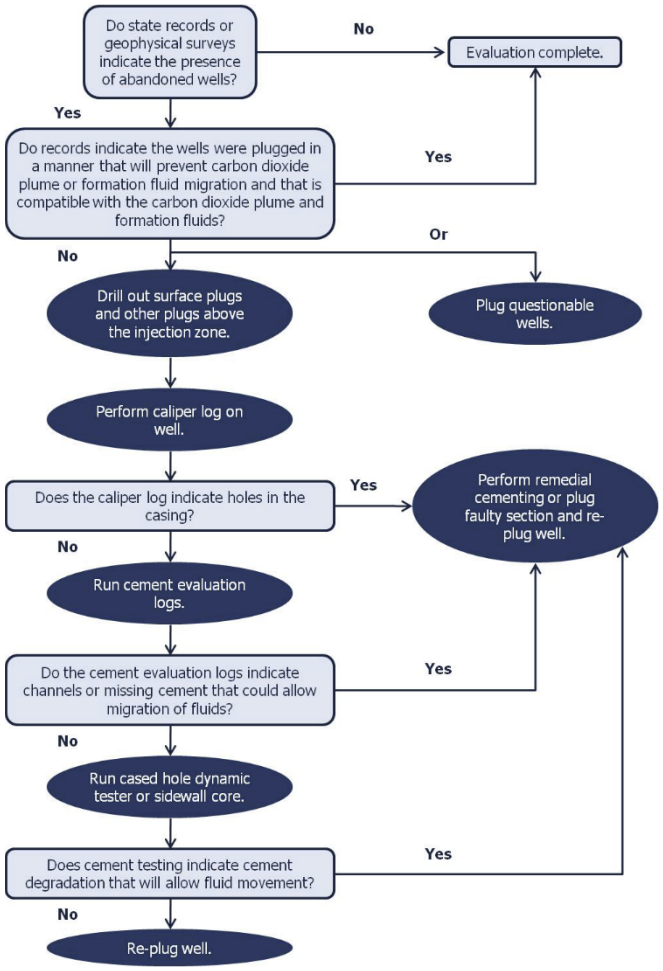

B.5.1.3 LEGACY WELLS REQUIRING CORRECTIVE ACTION

Based on the currently available information about the legacy wells in existence no corrective action is anticipated to be required. However, MC will evaluate and screen the wells identified in Appendix B-1 in more detail and has conservatively included potential corrective action for the one idle gas well and several other close deep wells within their financial responsibility plan.

B.5.2. PLAN FOR SITE ACCESS

At this time, MC does not anticipate the need to access any legacy wells for potential corrective action. However, MC is committed to obtaining such access agreements for any wells evaluated and determined to warrant corrective actions.

B.5.3. CORRECTIVE ACTION SCHEDULE

It is anticipated that any required deep well corrective actions would occur prior to the start of the Injection Period; therefore, no phased corrective actions are planned or contemplated at this time.

The scope and schedule for any future corrective actions resulting from a future AoR Re-evaluation will be developed in consultation with the US EPA UIC Program Director. Any such future corrective action will be performed after approval by the US EPA UIC Program Director.

B.6. RE-EVALUATION SCHEDULE AND CRITERIA

B.6.1. AoR RE-EVALUATION CYCLE

MC will re-evaluate the AoR at least once every 5 years (or when monitoring and operational conditions warrant) during the Injection and Post-Injection periods. For each re-evaluation, MC will:

1. Re-evaluate the AoR in the same manner specified in 40 CFR 146.84(c).
2. Identify all wells in the re-evaluated AoR that require corrective action in the same manner specified in 40 CFR 146.84(c).
3. Perform corrective action on wells requiring corrective action in the re-evaluated AoR in the same manner specified in 40 CFR 146.84(d).
4. Submit an amended Area of Review and Corrective Action Plan or demonstrate to the Program Director through monitoring data and modeling results that no amendment to the plan is needed. Any amendment to the Area of Review and Corrective Action Plan must be approved by the Program Director, must be incorporated into the permit, and are subject to the permit modification requirements at 40 CFR 144.39 or 40 CFR 144.41 as appropriate.

B.6.2. TRIGGERS FOR AoR RE-EVALUATIONS PRIOR TO THE NEXT SCHEDULED RE-EVALUATION

Triggers that may warrant an unscheduled re-evaluation of the AoR include:

- Significant changes in site operations that may alter model predictions and the AoR delineation. Examples of such changes include but are not limited to:
  - A change in the location or number of Class VI injection wells injecting into the same injection zone
  - A change in CO_2 injection rates or pressure outside of the limits of the original permit and AoR delineation
  - A material change in the composition of the injectate
- Monitoring results for the injected CO_2 plume and/or the associated pressure front that differ significantly from computational model predictions. Examples of such differences include but are not limited to:
  - Analysis of samples from IZMW-A1 indicating CO_2 concentrations materially greater than predicted by the computational model
  - Bottom-hole pressures for IZMW-A1 materially greater than predicted by the computational model
  - Significant micro-seismic activity outside the pressure front predicted by the computational model
- Obtaining new site characterization data that may significantly change model predictions and the delineated AoR. Examples of such data include but are not limited to:
  - Newly identified potential conduits for fluid movement
  - Updated information regarding injection or confining zone extent and thickness
  - Further characterization of formation heterogeneity

MC will discuss any such events with the UIC Program Director to determine if an AoR re-evaluation is required. If an unscheduled re-evaluation is triggered, MC will perform the steps described at the beginning of this section of this Plan.

B.7 REFERENCES

Aradóttir, E.S.P., E.L. Sonnenthal, G. Björnsson, and H. Jónsson, 2012. Multidimensional reactive transport modeling of CO_2 mineral sequestration in basalts at the Hellisheidi geothermal field, Iceland. *International Journal of Greenhouse Gas Control*, 9:24-40.

Asaka, M., Holt, R.M., Bakkt, A., 2021. Rock physics model of shale: predictive aspect, Journ. Geophys. Research, Solid Earth, 126, e2021JB021993.

Bandilla, K. W., Kraemer, S. R., and Birkholzer, J. T., 2012, Using semi-analytic solutions to approximate the area of potential impact for carbon dioxide injection, International Journal of Greenhouse Gas Control, vol. 8, p. 196-204.

Birkholzer, J.T., Cihan, A., Zhou, 2012, Impact-Driven Pressure Management Via Targeted Brine Extraction – Conceptual Studies of CO_2 Storage in Saline Formations, International Journal of Greenhouse Gas Control, vol. 7, p. 168-180

Brocher, T., 2004. Compressional and shear wave velocity versus depth in the San Francisco Bay Area, California: rules for USGS Bay Area velocity model 05.0.0, USGS Open file report 05-1317.

Cherven, V.B., 1983, Mesozoic through Paleogene evolution of the Sacramento basin, California, in Cherven, V.B. and Graham, S.A., eds., Geology and Sedimentology of the Southwestern Sacramento Basin and East Bay Hills: Field Trip Guidebook, Pacific Section, Society of Economic Paleontologists and Mineralogists, Los Angles, p. 21-31.

Crane, R.C., 1995, Geology of the Mt. Diablo region and East Bay hills, in Sangines, E.M., Andersen, D.E., and Buising, A.V., eds., Recent Geologic Studies in the San Francisco Bay Area: Pacific Section SEPM (Society for Sedimentary Geology), Volume 76, p. 87-114.

Division of Oil, Gas and Geothermal Resources (DOGGR), 1982a, California Oil and Gas Fields, Volume III – Northern California; Contour maps, cross sections and data sheets: California Department of Conservation, 330 p. (available from http://repository.usgin.org/category/place-keywords/california; last accessed 4/8/22)

Division of Oil, Gas, and Geothermal Resources (DOGGR) 1982b, Sherman Island gas field, *in* California Oil and Gas Fields, vol. III, Northern California: California Department of Conservation, Division of Oil and Gas, publication TR10.

Dobson, P.F., T.J. Kneafsey, S. Nakagawa, E.L. Sonnenthal, M. Voltolini, J.T. Smith, S.E. Borglin, 2021. Fracture sustainability in Enhanced Geothermal Systems: Experimental and modeling constraints. *J. Energy Resour. Technol.* 143, 100901.

Doughty, C. A., 2013, User's guide for hysteretic capillary pressure and relative permeability functionsin TOUGH2, Lawrence Berkeley National Laboratory, March.

Doughty, C., 2007, Modeling of geologic storage of carbon dioxide: comparison of non-hysteretic and hysteretic characteristic curves, Energy Conversion and Management, vol. 48(6), p. 1768-1781.

Finsterle, S., E.L. Sonnenthal, N. Spycher, 2014. Advances in subsurface modeling using the TOUGH suite of simulators. *Computers & Geosciences*, 65:2-12.

Foxall, W., Doughty, C., Lee, K.J., Nakagawa, S., Daley, T., Burton, E., Layland-Bachmann, C., Borglin, S., Freeman, K., Ajo-Franklin, J., Jordan, P., Kneafsey, T., Oldenburg, C., Ulrich, C., 2017. Investigation of Potential Induced Seismicity Related to Geologic Carbon Dioxide Sequestration in California, Final Project Report. report to California Energy Commission, Energy Research and Development Division, CEC-500-2017-028, Sacramento, California.

Graham, S.A., Gavigan, C., McCloy, C., Hitzman, M., Ward, R., and Turner, R., 1983, Basin evolution during the change from convergent to transform continental margin: an example from the Neogene of California, in Cherven, V.B., and Graham, S.A., eds., 1983, Geology and Sedimentology of the Southwestern Sacramento Basin and East Bay Hills: Field Trip Guidebook, Pacific Section, Society of Economic Paleontologists and Mineralogists, Los Angles, p. 101-118.

Ingersoll, R. V., and Dickinson, W. R., 1981, Great Valley Group (sequence), Sacramento Valley, California, in Frizzell, V., ed., Upper Mesozoic Franciscan rocks and Great Valley sequence, central Coast ranges, California (Annual Meeting, Pacific Section SEPM field trips 1 and 4): Pacific Section, Society of Economic Paleontologists and Mineralogists, p. 1–33.

Kim, J., Sonnenthal, E.L., and Rutqvist, J., 2012. Formulation and sequential numerical algorithms of coupled fluid/heat flow and geomechanics for multiple porosity materials, *Int. J. Numer. Meth. Engng.*, 92, 425-456

Krug, E.H., Cherven, V.B., Hatten, C.W., Roth, J.C., 1992, Subsurface structure in the Montezuma Hills, southwestern Sacramento basin, in Cherven, V.B., and Edmondson, W.F., eds., Structural Geology of the Sacramento Basin: Volume MP-41, Annual Meeting, Pacific Section, Society of Economic Paleontologists and Mineralogists, p. 41-60.

Lai, M., 1999. Shale stability: drilling fluid interaction and shale strength, 1999 SPE Latin American and Caribbean Petroleum Engineering, Caracas, Venezuela.

MacKevett, N.H., 1992, The Kirby Hills fault zone, in Cherven, V.B., and Edmondson, W.F., eds., Structural Geology of the Sacramento Basin: Volume MP-41, Annual Meeting, Pacific Section, Society of Economic Paleontologists and Mineralogists, p. 61-78.

Myer, L., L. Chiaramonte, T. M. Daley, D. Wilson, W. Foxall, J. H. Beyer, 2010, Potential for Induced Seismicity Related To The Northern California CO_2 Reduction Project Pilot Test, Solano County, California, LLNL-TR-435831 June 15.

Narasimhan, T. N. and Witherspoon, P. A. 1976. An Integrated Finite Difference Method for Analyzing Fluid Flow in Porous Media. *Water Resources Research*, 12(1), 57-64.

Nicot, J. P., Oldenburg, C. M., Brynt, S. L., and Hovorka, S. D., 2008, Pressure perturbation from geologic carbon sequestration: Area-of-review boundaries and borehole leakage driving forces. Energy Procedia.

Oldenburg, Curtis M. and Preston D. Jordan, 2017, Long-Term Viability of Underground Natural Gas Storage in California, An Independent Review of Scientific and Technical Information, California Council on Science and Technology December.

Pan, L., Spycher, N., Doughty, C., and Pruess, K. 2015. ECO2N V2.0: A TOUGH2 fluid property module for mixtures of water, NaCl, and CO_2. Earth Sciences Division, Lawrence Berkeley National Laboratory, University of California, Berkeley. LBNL-6930E. February.

Pasquini, D.E., and Milligan, H.L., 1967, Correlation Section 15, Sacramento Valley, Suisun Bay to Lodi: Pacific Section, American Association of Petroleum Geologists.

Peaceman, D. W., 1977, Interpretation of well-block pressures in numerical reservoir simulation, SPE 6893, 52nd Annual Fall Technical Conference and Exhibition, Denver, 1977.

Pratt, H. R., W. A. Hustrulid, and D. E. Stephenson, 1978, Earthquake Damage to Underground Facilities, Environmental Transport Division, November.

Pruess, K., Oldenburg, C., and Moridis, G., 2012, TOUGH2 User's Guide, Version 2, Earth Sciences Division, Lawrence Berkeley National Laboratory, University of California, Berkeley. LBNL-43134. September

Pruess, K., Garca, J., Kovscek, T., Oldenburg, T. C., Rutqvist, J., Steefel, C., & Xu, T., 2004, Code intercomparison builds confidence in numerical simulation models for geologic disposal of CO_2, Energy, vol. 29(9-10), p. 1431-1444.

Pruess, K., Oldenburg, C., and Moridis, G., 2011, TOUGH2 User's Guide.

Pruess, K., and Spycher, N., 2007, ECO2N – A fluid property module for the TOUGH2 code for studies of CO_2 storage in saline aquifers, Energy Conversion and Management, vol. 48, p. 1761-1767.

Smith, J.T., Sonnenthal, E.L., and Cladouhos, T., 2015. Thermal-Hydrological-Mechanical Modelling of Shear Stimulation at Newberry Volcano, Oregon. *Proceedings of 49th US Rock Mechanics/Geomechanics Symposium*, American Rock Mechanics Association, ARMA 15-0680.

Sonnenthal, E., N. Spycher, T. Xu, and L. Zheng, 2021. TOUGHREACT V4.12-OMP and TReactMech V1.0 Geochemical and Reactive-Transport User Guide. LBNL Report 2001410. https://tough.lbl.gov/software/toughreact.

Sonnenthal, E., W. Pettitt, T. Smith, A. Riahi, D. Siler, E. Majer, P. Dobson, B. Ayling, B. Damjanac, 2018. Continuum thermal-hydrological-mechanical modeling of the Fallon FORGE Site, GRC Transactions, 42, 10 p.

Spycher, N., and Pruess, K., 2005, Carbon dioxide-water mixtures in geologic sequestration of carbon dioxide. II. Partitioning in chloride brines at 12-100 degrees Celsius and up to 600 bar. Geochemical et Cosmochimica Acta, vol. 69, p. 3309-3320.

Segall, P. (1989), Earthquakes triggered by fluid extraction, Geology, 17, 942–946.

Sloan, D., Schwartz, D., and Unruh, J., Regional Geology of Mount Diablo, California: Its Tectonic Evolution on the North American Plate Boundary: Geological Society of America Memoir 217, p. 179-200.

Suckale, J. (2009), Induced seismicity in hydrocarbon fields, Adv. Geophys., 51, 55–106.

Sullivan, R., Sullivan, M.D., Dedmon, P., and Edwards, S.W., 2021a, The occurrence and mining of coal and sand deposits in the Middle Eocene Domengine Formation of the Mount Diablo Coalfield, California, in Sullivan, R., Sloan, D., Schwartz, D., and Unruh, J., Regional Geology of Mount Diablo,

California: Its Tectonic Evolution on the North American Plate Boundary: Geological Society of America Memoir 217, p. 65-95.

Sullivan, R., Sullivan, M.D., Edwards, S.W., Sarna-Wojicicki, A., Hackworth, R.A., Deino, A.L., 2021b, The mid-Cenozoic succession on the northeast limb of Mount Diablo anticline, California-a stratigraphic record of tectonic events in the forearc basin, in Sullivan, R., Sloan, D., Schwartz, D., and Unruh, J., Regional Geology of Mount Diablo, California: Its Tectonic Evolution on the North American Plate Boundary: Geological Society of America Memoir 217, p. 269-303.

United States Environmental Protection Agency (EPA). 2013. UIC Program Class VI Well Area of Review Evaluation and Corrective Action Guidance. EPA 816-R-13-005.

Unruh, J.R., and Hector, S.T., 1999, Subsurface Characterization of the Potrero-Ryer Island Thrust System, Western Sacramento-San Joaquin Delta, Northern California: Final Technical Report submitted to the U.S. Geological Survey, National Earthquake Hazards Reduction Program award number 1434-HQ-96-GR-02724, 32 p.

Unruh, J., Hitchcock, C., Blake, K., and Hector, S., 2016, Characterization of the Southern Midland Fault in the Sacramento-San Joaquin Delta, in Ferriz, H. and Anderson, R., eds., Applied Geology in California: Association of Engineering Geologists, Special Publication 26, p. 757-776.

Unruh, J., 2021, Upper plate deformation during blueschist exhumation, ancestral western California forearc basin, from stratigraphic and structural relationships at Mount Diablo and in the Rio Vista Basin, in Sullivan, R.,

Walsh, F.R., and Zoback, M.D., 2015, Oklahoma's recent earthquakes and saltwater disposal: Science Advances, v. 1, e1500195, doi:10.1126 /sciadv.1500195.

Xu, T., N. Spycher, E. Sonnenthal, G. Zhang, L. Zheng, and K. Pruess, 2011. TOUGHREACT Version 2.0: A simulator for subsurface reactive transport under non-isothermal multiphase flow conditions. Computers & Geosciences, 37:763–774.

Zhai, G., M. Shirzaei, and M. Manga (2021) Widespread deep seismicity in the Delaware Basin, Texas, is mainly driven by shallow wastewater injection, PNAS, vol. 118, e2102338118.

APPENDIX B-1

OIL AND GAS WELLS

APPENDIX B-1. OIL AND GAS WELL LOCATIONS IDENTIFIED WARRANTING DETAILED EVALUATION FOR POTENTIAL FUTURE CORRECTIVE ACTIONS

Well ID (API No.)	Well Name	Well Number	Spud Date	Completion date	Abandonment Date	Well (CalGEM) Type	CalGEM Status	Latitude	Longitude	Miles from Proposed IW-A1	O.H. TD	Top Meganos (M.D.)	Conductor Pipe	Surface Casing	Intermediate	Production String	Shallow Plug	Fresh Water Plug	Deeper Plug 1	Deeper Plug 2	Deeper Plug 3	Deeper Plug 4	Comments
06700295	Signal-R.I.L. Co	1	4/22/1965	5/11/1965	5/11/1965	Dry Hole	Plugged	38.045319	-121.775177	5.3	8,835	7642	16" @ 40'	9-5/8" @ 800'	none	none	10' to surface	850' to 756', 55 sx cmt					This well has no pipe string reaching the top Meganos
06720166	Lower Sherman Island	1	11/8/1980	12/1/1980	12/1/1980	Dry Hole	Plugged	38.05101	-121.78112	4.8	8.595	7899	not listed	8-5/8" @ 904'	none	none	60' to surface	560' (109 cu.ft. cmt.)	960' (115 cu.ft. cmt.)				This well has no pipe string reaching the top Meganos
09420724	McDougal	2-8	6/19/1985	8/7/1985	8/12/1985	Dry Hole	Plugged	38.114178	-121.88942	2.6	12,191	8350	not listed	13-3/8" @ 722'	9-5/8" @ 7173'	none	90' to surface (55 cu.ft.)	1301' (81 cu.ft.)					This well has no pipe string reaching the top Meganos
09500005	Turner	1	10/16/1966	11/11/1966	11/16/1966	Dry Hole	Plugged	38.179634	-121.866234	6.5	10,449	8395	not listed	10-3/4" @ 1025	none	none	4'-14'	2050'-1854', 1085'-925'					This well has no pipe string reaching the top Meganos
09500095	Stewart	74-7	7/18/1943	9/4/1943	9/4/1943	Dry Hole	Plugged	38.206974	-121.90081	8.7	4,189	4103	not listed	11-3/4" @ 500'	none	none	0'-110' 6-5/8" water well	718' to 580' (100 sx.)					This well has no pipe string reaching the top Meganos
09500426	Dozier-Pressley	1	8/19/1965	9/13/1965	9/14/1965	Dry Hole	Plugged	38.119598	-121.774117	3.6	10,503	7030	not listed	9-5/8" @ 1009'	none	none	10' to surface	1070'-912' (75 sx.)					This well does have pipe reaching Top Meganos
09520017	Sumpf-Williams-Turner	2	6/9/1967	7/22/1967	3/1/1968	Dry Hole	Plugged	38.181805	-121.866241	6.7	12,216	8406	16" @ 80'	10-3/4" @ 2009'	7" @ 8747'	4-1/2" @ 12,193'	10' to surface	2730'-2773' (35 sx.)	3734'-3860' in OH for RD	7705'-7750' in RD	7750'-7850' in RD		Meganos reached in Original Hole but not in Redrill, which was completed as a gas well
09520021	Feykert	1	7/7/1967	9/26/1967	9/18/1966	Dry Gas	Plugged	38.05803	-121.881	2.3	11,040	9292 (in O.H.)	16" @ 70'	10-3/4" @ 1500'	none	4-1/2" @ 7750'	50' to surface	300' plug inside tubing	6713'-6804' (50 sx.)				This well has no pipe string reaching the top Meganos
09520080	Sumpf-Williams O'Brien	1	12/11/1968	1/19/1969	2/4/1969	Dry Hole	Plugged	38.180275	-121.874733	6.7	10,600	8190	not listed	11-3/4" @ 507'	8-5/8" @ 6773'	none	10' to surface	457'497' (65 sx.)	12,990'-13,150' (71 sx.)				This well does have pipe reaching Top Meganos
09520430	Anderson	1-5	7/26/1980	11/2/1980	12/31/1980	Dry Hole	Plugged	38.136429	-121.774445	5.8	14,269	7390	not listed	13-3/8" @ 1499'	none	13-3/8" @ 13,183'	5'-50' (38 sx.)	1021'-1515' (300 sx.)	1322'-1792' (218 sx.)				This well has no pipe string reaching the top Meganos
09520436	GP	1-7	8/8/1980	9/5/1980	9/7/1980	Dry Hole	Plugged	38.1157	-121.804878	3.6	11,000	8383	not listed	9-5/8" @ 1050'	none	none	surface plug	1001'-1099' (57 s..)					This well has no pipe string reaching the top Meganos
09520450	Neil	1	2/22/1981	3/17/1981	3/19/1981	Dry Hole	Plugged	38.122238	-121.787041	4.7	9,600	7500	not listed	9-5/8" @ 1022'	none	none	60' to surface (50 sx.)	718'-1088' (200 sx.)	2059'-1938' (35 sx.)	7004'-6804' (156 sx.)	8567'-8315' (134 sx.)	9327'-9128' (71 sx.)	This well has no pipe string reaching the top Meganos
09520674	Swepi-Hershey State	1-8	6/17/1984	7/22/1984	7/26/1984	Dry Hole	Plugged	38.114487	-121.888824	2.6	9,328	8170	30" @ 80'	20" @ 518'	13-3/8" @ 2038'	9-5/8" @ 6977'	140' to surface (50 sx.)	1350'-950' (159 sx.)	957'-765' (72 sx.)	6939'-6610' (100 sx.)			This well has no pipe string reaching the top Meganos
09520697	Dozier & Pressley	1-9	9/25/1984	10/7/1994	10/8/1984	Dry Hole	Plugged	38.121239	-121.766487	5.6	7,307	6589	not listed	8-5/8" @ 907'	none	none	60' to surface (11 sx.)	405'-205' (72 sx.)	1675'-1545' (92 cu.ft.)	7218'-6835' (173 cu.ft.)			This well has no pipe string reaching the top Meganos
09520750	McGraugh	1-22	3/20/1986	4/18/1986	10/21/1988	Dry Gas	Plugged	38.182125	-121.858559	6.7	10,595	8563	not listed	10-3/4" @ 2026'	none	5-1/2" @ 10,876'	30' to surface	1169'-919' (120 sx.)	1884'-2055' (120 sx.)	9184'-9314' (50 sx.)			This well does have pipe reaching Top Meganos
09520878	Dozier-Pressley	1	5/2/1990	5/13/1990	5/14/1990	Dry Hole	Plugged	38.098106	-121.767044	5.1	8,500	7125	16" @ 53.5'	8-5/8" @ 854'	none	none	60' to 20' (20 sx.)	904'-630' (100 sx.)					This well has no pipe string reaching the top Meganos
09520963	Gunn	1	7/23/1993	8/19/1993	8/20/1993	Dry Hole	Plugged	38.195755	-121.88681	7.8	9,310	6598	no listed	8-5/8" @ 1070'	none	none	30' to surface	900'-700'+-	1122'-1000' (70 cu.ft.)				This well has no pipe string reaching the top Meganos
09521120	R.W. Blacklock	1-21	7/2/2001	10/3/2001	6/10/2003	Dry Gas	Plugged	38.172028	-121.876274	6.1	11,544	7910	not listed	13-3/8" @ 833'	9-5/8" @ 7953'	4-1/2" @ 11,226'	25 lineal feet at surface	1500'-1755' (105 sx.)	9514'-10,400' (50 sx.)				This well does have pipe reaching Top Meganos
09521228	Roaring River	20-2	7/29/2005	10/3/2005	Idle	Dry Gas	Idle	38.07228	-121.887	1.9	10,301	unknown	not listed	16" @ 320'	10-3/4" @ 3013'	7" @ 9085'							Meganos likely reached in this well, but e-log was not run in lower part of hole. E-log run to 8040'.

APPENDIX B-2

WATER WELLS

TABLE B-2. WATER WELLS WITHIIN THE AREA OF REVIEW

WCR Number	Latitude	Longitude	Section	Township	Range	Date Work Ended	Total Depth	Top of Screen	Bottom of Screen	Casing Size	Planned Use	Drilling Company
WCR2012-00374	38.115278	-121.823889					200	60	200	5"	Agricultural & Irrigation	Pacific Coast Well and Pump, inc.
WCR1990-013060	38.089167	-121.889444				9/20/1990	325				Cathodic Protection	American Construction & Supply
WCR2007-000083	38.14787	-121.88926	32	T4N	R1E		250	125	250	2"	Cathodic Protection	Farwest Corrosion Control
WRC2019-013918	38.140959	-121.866744	33	T4N	R1E	10/1/2019	420				Cathodic Protection	American Construction and Supply Inc.
WCR2021-012625	38.147535	-121.872885	33	T4N	R1E	9/29/2021	300				Cathodic Protection	CorrproCompanies, Inc.
WCR2011-005762	38.138889	-121.808333	1	T3N	R1E	11/17/2011	320	270	310	6"	Domestic	DeJesus Pump Well Drilling
WCR0047180	38.132778	-121.834167	2	T3N	R1E	10/14/1981	149			6.625"	Domestic	Vaca Drilling Co.
WCR1988-007782	38.132778	-121.834167				9/20/1988	260			6"	Domestic	Vaca Drilling Co.
WCR1991-004184	38.132778	-121.8525	3	T3N	R1E	9/7/1991	220	25	220	5"	Domestic	Vaca Drilling Co.
WCR2010-001159	38.13289	-121.85243					400	360	400	6"	Domestic	Woodward Drilling Co.
WCR1994-000929	38.13243	-121.85243				4/3/1994	120			5"	Domestic	Vaca Drilling Co.
WCR1982-001391	38.13296	-121.87098	4	T3N	R1E	8/12/1982	100				Domestic	Vaca Drilling Co.
WCR2010-001149	38.13296	-121.87098				10/27/2010	295			6"	Domestic	A&A Gross Drilling
WCR1991-000769	38.13296	-121.87098				5/22/1991	65			6"	Domestic	Carter Water Well Drilling
WCR1997-005860	38.13206	-121.87098				10/23/1997	240	78	254	5"	Domestic	Vaca Drilling Co.
WCR1997-005863	38.13296	-121.87098				9/22/1997	200	60	200	5"	Domestic	Vaca Drilling Co.
WCR1956-000526	38.13296	-121.87098				6/24/1956	60	40	60	6"	Domestic	Vaca Drilling Co.
WCR1975-00464	38.11839	-121.87108				8/27/1975	221	25	220		Domestic	Vaca Drilling Co.
WCR1989-010443	38.11825	-121.83391	11	T3N	R1E	7/17/1989	200			5"	Domestic	Vaca Drilling Co.
WCR1975-000465	38.11816	-121.81562	12	T3N	R1E		120	40	120	5"	Domestic	Vaca Drilling Co.
WCR1986-004919	38.089167	-121.889444	20	T3N	R1E	6/23/1986	101			5"	Domestic	Vaca Drilling Co.
WCR1954-000264	38.08922	-121.85223				not listed	210	70	210	6"	Domestic	Vaca Drilling Co.
WCR1980-001076	38.07717	-121.83229	26	T3N	R1E	12/16/1980	100			5"	Domestic	Vaca Drilling Co.
WCR1982-001399	38.078056	-121.852778				9/27/1982	100			5"	Domestic	Vaca Drilling Co.
WCR1954-000265	38.08925	-121.87124	21	T3N	R1E						Domestic	Vaca Drilling Co.
WCR1973-000801	38.19149	-121.88893	17	T4N	R1E	4/22/1973	121	60	110	5"	Domestic Water Supply	Vaca Drilling Co.
WCR1957-000159	38.19149	-121.88893	17	T4N	R1E	1/30/1957	60	31	59	6"	Domestic Water Supply	H. O. Krossa
WCR1986-004937	38.176944	-121.888889	20	T4N	R1E	8/7/1986				5"	Domestic Water Supply	Vaca Drilling Co.
WCR1974-000407	38.176944	-121.888889	20	T4N	R1E	7/23/1974	142	30	140	6"	Domestic Water Supply	Vaca Drilling Co.
WCR2006-000681	38.17682	-121.889	20	T4N	R1E	6/18/2006	280	55	280	5"	Domestic Water Supply	Vaca Drilling Co.
WCR1991-004174	38.17682	-121.889	20	T4N	R1E	6/20/1991	140	100	140	5"	Domestic Water Supply	Vaca Drilling Co.
WCR1978-000121	38.176667	-121.852222	22	T4N	R1E	10/13/1978	247	70	240		Domestic Water Supply	Vaca Drilling Co.
WCR2001-003995	38.17658	-121.85225	22	T4N	R1E	5/16/2001	260	100	260	5"	Domestic Water Supply	Vaca Drilling Co.
WCR1977-002210	38.16182	-121.81567	25	T4N	R1E	11/3/1977	103	80	100	5"	Domestic Water Supply	Vaca Drilling Co.
WCR1997-005864	38.16182	-121.81567	25	T4N	R1E	9/28/1997	260	120	260	5"	Domestic Water Supply	Vaca Drilling Co.
WCR1982-002019	38.1619	-121.83401	26	T4N	R1E	1/1/1982	174			9"	Domestic Water Supply	Seebeck

TABLE B-2. WATER WELLS WITHIIN THE AREA OF REVIEW

WCR Number	Latitude	Longitude	Section	Township	Range	Date Work Ended	Total Depth	Top of Screen	Bottom of Screen	Casing Size	Planned Use	Drilling Company
WCR1985-000470	38.1619	-121.83401	26	T4N	R1E	11/4/1985	181			5"	Domestic Water Supply	Vaca Drilling Co.
WCR1985-000454	38.16236	-121.8891	29	T4N	R1E	9/22/1985	101			6"	Domestic Water Supply	Vaca Drilling Co.
WCR1999-005850	38.16236	-121.8891	29	T4N	R1E	10/19/1999	120			5"	Domestic Water Supply	Vaca Drilling Co.
WCR1974-00406	38.16236	-121.8891	29	T4N	R1E	7/22/1974	121	50	120	6"	Domestic Water Supply	Vaca Drilling Co.
WCR2006-000682	38.16236	-121.8891	29	T4N	R1E		150	30	150	5"	Domestic Water Supply	Vaca Drilling Co.
WCR1990-000913	38.16236	-121.8891	29	T4N	R1E	6/26/1990	120			6"	Domestic Water Supply	Carter Water Well Drilling Service
WCR2008-001635	38.14759	-121.87084	33	T4N	R1E		300	160	300	6"	Domestic Water Supply	A&A Gross Drilling
WCR1997-005866	38.147222	-121.834167	35	T4N	R1E	10/23/1997	260			5"	Domestic Water Supply	Vaca Drilling Co.
WCR2007-001716	38.14726	-121.8158	36	T4N	R1E	10/24/2007	200	160	200	5"	Domestic Water Supply	Vaca Drilling Co.
WCR2007-001717	38.14726	-121.8158	36	T4N	R1E	10/29/2007	220	40	220	5"	Domestic Water Supply	Vaca Drilling Co.
WCR1951-000551	38.14726	-121.8158	36	T4N	R1E		28	21	28	6"	Domestic Water Supply	Owner of Well
WCR2022-009774	38.12338	-121.79065	7	T3N	R2E		350	240			Domestic Water Supply	Martell Water Systems, Inc.
WCR2011-006952	38.104722	-121.765556	16	T3N	R2E	12/22/2011	79	50	79	4"	Domestic Water Supply	Woodward Drilling Co.
WCR2022-009219	38.10821	-121.79255	18	T3N	R2E	8/6/2022	330				Domestic Water Supply	Martell Water Systems, Inc.
WCR1988-007783	38.089722	-121.761111	21	T3N	R2E	9/22/1988	140			5"	Domestic Water Supply	Vaca Drilliing Co.
WCR1987-008321	38.0708	-121.75806	28	T3N	R2E	1/8/1987	330			6"	Domestic Water Supply	Keith Gross
WCR1990-006514	38.073234	-121.757705				4/19/1999	221	145	215	6"	Domestic Water Supply	Universal Pump Company
WCR2008-004358	38.073582	-121.756927				4/28/2008	400	335	400		Domestic Water Supply	DeJesus Pump Well Drilling
WCR1998-002151	38.0703588	-121.755855				7/16/1998	460	220	420	6"	Domestic Water Supply	Martell Water Systems, Inc.
WCR2013-000268	38.072778	-121.7575				12/12/2013	415	355	415	6"	Domestic Water Supply	A&A Gross Drilling
WCR1990-006515	38.073234	-121.757705				4/19/1990	221	185	215	8"	Domestic Water Supply	Universal Pump Company
WCR1978-000687	38.0708	-121.75806				7/23/1978	405				Domestic Water Supply	Alisto Engineering Group
WCR2006-003552	38.0708	-121.75806				10/5/2006	500	170	190	6"	Domestic Water Supply	DeJesus Pump Well Drilling
WCR2020-010297	38.073402	-121.755669				8/7/2020	480	440	470		Domestic Water Supply	Diversified Pump & Well
WCR1992-002169	38.072933	-121.75732				4/16/1992	412			6"	Domestic Water Supply	A&A Gross Drilling
WCR2008-006673	38.072559	-121.758157				2/12/2008	480	320	440		Domestic Water Supply	DeJesus Pump Well Drilling
WCR1978-000682	38.071944	-121.759167					405				Domestic Water Supply	Alisto Engineering Group
WCR2008-005505	38.073167	-121.756796				1/14/2008	400	350	400		Domestic Water Supply	DeJesus Pump Well Drilling
WCR2014-003312	38.074688	-121.753441				3/27/2014	195	175	195	6"	Domestic Water Supply	Martell Water Systems, Inc.
WCR2009-00412	38.072653	-121.757947					400	360	400	6"	Domestic Water Supply	A&A Gross Drilling
WCR0079860	38.074277	-121.755372				1/18/1987	280	260	280	6"	Domestic Water Supply	A&A Gross Drilling
WCR2013-000393	38.072778	-121.757778				12/2/2013	420			6"	Domestic Water Supply	A&A Gross Drilling
WCR2017-00593	38.072447	-121.758378				2/20/2017	460	320	420		Domestic Water Supply	Diversified Pump & Well
WCR2016-009676	38.071944	-121.778333	29	T3N	R2E	12/8/2016	150	50	150	5"	Domestic Water Supply	Pacific Coast Well & Pump Inc.
WCR1998-000420	38.051399	-121.779921	5	T2N	R2E	12/9/1998	300	73	93	6"	Domestic Water Supply	DeJesus Pump Well Drilling
WCR2002-00456	38.07504	-121.87184	28	T3N	R1E	6/6/2002	80	24	64	10"	Industrial Water Supply	Gregg Drilling and Testing

TABLE B-2. WATER WELLS WITHIIN THE AREA OF REVIEW

WCR Number	Latitude	Longitude	Section	Township	Range	Date Work Ended	Total Depth	Top of Screen	Bottom of Screen	Casing Size	Planned Use	Drilling Company
WCR2002-00460	38.07504	-121.87184				6/6/2002	80	20	50	10"	Industrial Water Supply	Gregg Drilling and Testing
WCR2002-00458	38.07504	-121.87184				6/6/2002	80	20	70	10"	Industrial Water Supply	Gregg Drilling and Testing
WCR2002-00457	38.07504	-121.87184				6/6/2002	80	26	66	10"	Industrial Water Supply	Gregg Drilling and Testing
WCR2002-00459	38.07504	-121.87184				6/6/2002	50	20	50	10"	Industrial Water Supply	Gregg Drilling and Testing
WCR2002-000461	38.07504	-121.87184				6/6/2002	80	20	50	10"	Industrial Water Supply	Gregg Drilling and Testing
WCR2002-000463	38.07504	-121.87184				6/6/2002	53	15	20	10"	Industrial Water Supply	Gregg Drilling and Testing
WCR2002-000452	38.07504	-121.87184				6/6/2002	78	34	44	10"	Industrial Water Supply	Gregg Drilling and Testing
WCR2002-000462	38.07504	-121.87184				6/6/2002	50	18	50	10"	Industrial Water Supply	Gregg Drilling and Testing
WCR2002-000453	38.07504	-121.87184				6/6/2002	70	34	64	10"	Industrial Water Supply	Gregg Drilling and Testing
WCR2008-006212	38.1875	-121.875	16	T4N	R1E		243	97	117	6"	Irrigation & Agriculture	not listed
WCR1981-003176	38.1328	-121.83408				10/14/1981	150			9"	Irrigation-Agriculture	Seebeck Drilling
WCR1057-000039	38.08922	-121.85223				1/15/1957	773	100	773	13"	Irrigation-Agriculture	Eaton Drillng Co.
WCR2017-009371	38.12778	-121.794722	7	T3N	R2E		350	270	350	6"	Irrigation-Agriculture	A&A Gross Drilling
WCR1951-000614	38.11813	-121.76054	9	T3N	R2E	4/22/1951	610	226	610	12"	Irrigation-Agriculture	Layne-Western Company, Inc.
WCR1991-004186	38.089167	-121.779167	20	T3N	R2E	9/3/1991	220	30	220	5"	Irrigation-Agriculture	Vaca Drilliing Co.
WCR1990-006515	38.0708	-121.75806				4/19/1990	221	185	215		Irrigation-Agriculture	Calwater Drilling Co.
WCR1997-000703	38.05494	-121.782631	31	T3N	R2E	9/28/1997	705	123	223	6"	Irrigation-Agriculture	Martell Water Systems, Inc.
WCR1990-002058	38.0708	-121.75806				1/11/1990	250			6"	No data	No data
WCR1990-002057	38.072559	-121.758157				1/11/1990	190			6"	No data	No data
WCR2013-003785	38.074983	-121.753821				11/12/1989	190			5"	No data	No data
WCR1990-007610	38.0708	-121.75806				5/14/1990	195			6"	No data	No data
WCR1989-003822	38.0708	-121.75806				12/27/1989	160			6"	No data	No data
WCR1956-000180	38.05969	-121.7775	32	T3N	R2E	3/4/1956	84				No data	No data
WCR1944-000022	38.08922	-121.85223	22	T3N	R1E	9/22/1944	750				not listed	R. L. Norris and Son
WCR1944-000024	38.08922	-121.85223				9/22/1944	250				not listed	R. L. Norris and Son
WCR1776-000682	38.08922	-121.85223					510				not listed	Western Well Drilling Co.
WCR1776-00683	38.07504	-121.87184				not listed	148				not listed	not listed
WCR1776-000684	38.07464	-121.88954	29	T3N	R1E	not listed	142				not listed	not listed
WCR1986-007479	38.162222	-121.889167	29	T4N	R1E		150			5"	not listed	not listed
WCR007368	38.13271	-121.81576				not listed					not listed	not listed
WCR0278803	38.07504	-121.87184				not listed					Other Unknown	not listed
WCR0326030	38.0708	-121.75806					310				Other unknown	A&A Gross Drilling
WCR0116118	38.074102	-121.754704				10/5/2006	190	170	190	6"	Other Unknown	DeJesus Pump Well Drilling
WCR1998-002152	38.073588	-121.755855				6/24/1998					Other Unused	Martell Water Systems, Inc.
WCR1978-000136	38.17658	-121.85225	22	T4N	R1E	12/8/1978	260	60	259	5"	Other-not specified	Vaca Drilling Co.
WCR2000-000485	38.0708	-121.75806				6/29/2000	520	200	290	6"	Public Water Supply	DeJesus Pump Well Drilling

TABLE B-2. WATER WELLS WITHIIN THE AREA OF REVIEW

WCR Number	Latitude	Longitude	Section	Township	Range	Date Work Ended	Total Depth	Top of Screen	Bottom of Screen	Casing Size	Planned Use	Drilling Company
WCR1776-000066	38.08922	-121.85223				not listed	312				Public Water Supply	not listed
WCR1990-004026	38.07817	-121.85294	27	T3N	R1E	3/28/1990	300	240	300	6"	Public Water Supply	Ronald L. Clark
WCR2022-009221	38.107686	-121.791583	18	T3N	R2E	8/8/2022	18				Stock and Animal Watering	Martell Water Systems, Inc.
WCR1995-003844	38.17682	-121.889	20	T4N	R1E	6/25/1995	140	40	140	5"	Water Supply	Vaca Drilling Co.
WCR1989-011954	38.16199	-121.85237	27	T4N	R1E	11/2/1989	180			5"	Water Supply	Vaca Drilling Co.
WCR1989-011955	38.14746	-121.85252	34	T4N	R1E	11/3/1989	140			5"	Water Supply	Vaca Drilling Co.
WCR1981-003162	38.103611	-121.833889	14	T3N	R1E	6/14/1981	78			7"	Water Supply	Seebeck Drilling
WCR1994-000935	38.13289	-121.85243				4/18/1994						Vaca Drilling Co.
WCR1991-00768	38.125556	-121.876389	9	T3N	R1E	4/30/1991	125			6"		
WCR1924-00004	38.10383	-121.88956										